

# Advances and Trends in Chemically Doped Graphene

Sami Ullah, Qitao Shi, Junhua Zhou, Xiaoqin Yang, Huy Q. Ta, Maria Hasan, Nasir Mahmood Ahmad, Lei Fu, Alicja Bachmatiuk, and Mark H. Rümmeli\*

Chemically doped graphene materials are fascinating because these have different desirable attributes with possible synergy. The inert and gapless nature of graphene can be changed by adding a small number of heteroatoms to substitute carbon in the lattice. The doped material may display superior catalytic activities; durable, fast, and selective sensing; improved magnetic moments; photoresponses; and activity in chemical reactions. In the current review, recent advances are covered in chemically doped graphene. First, the different types of heteroatoms, their bonding configurations, and briefly their properties are discussed. This is followed by the description of various synthesis and analytical methods essential for assessing the characteristics of heterographene with specific focus on the selected graphene materials of different dopants (particularly, single dopants, including N, B, S, P, first three halogens, Ge, and Ga, and codopants, such as N/O), and more importantly, up-to-date applications enabled by the intentional doping. Finally, outlook and perspectives section review the existing challenges, future opportunities, and possible ways to improve the graphitic materials. The goal is to update and inspire the readers to establish novel doped graphene with valuable properties and for current and futuristic applications.

conductivity, eminent mechanical strength, amazing chemical stability, flexibility, light weight, large surface area, matchless thinness, and transparency all in one material.<sup>[1–3]</sup> It has been extensively explored in 0–3D (e.g., graphene quantum dots (GQDs), carbon nanotubes, and porous graphene), in many functionalized forms, as well as in combination with other materials (composites).<sup>[4–9]</sup> The typical goals are as follows: 1) exploit the unique behavior of graphene; 2) overcome the gapless symmetry of graphene as a zero bandgap material (i.e., the conduction and valence states meet at some point) that hinders its use in the electronic industry; 3) enhance the reactivity of graphene, which is naturally stable under ambient conditions owing to the delocalized  $\pi$ -electron system that resists chemical modifications, for use in synthetic industry; and 4) design new materials with ideal attributes.<sup>[10–15]</sup>

Among the graphene derivatives, a focus area is chemically doped graphene—more specifically covalently doped graphene, in which a controlled number of foreign atoms (heteroatoms) are intentionally introduced to customize the properties of graphene. The potential uses of chemically doped graphene include:

## 1. Introduction

Since its isolation, graphene is often called a substance of wonder due to its notable features, such as improved

S. Ullah, Q. Shi, J. Zhou, X. Yang, Prof. A. Bachmatiuk, Prof. M. H. Rümmeli  
College of Energy Soochow Institute for Energy and Materials Innovations  
Soochow University  
Suzhou 215006, China  
E-mail: mhr1@suda.edu.cn

S. Ullah, Q. Shi, J. Zhou, X. Yang, Prof. A. Bachmatiuk, Prof. M. H. Rümmeli  
Key Laboratory of Advanced Carbon Materials and Wearable Energy Technologies of Jiangsu Province  
Soochow University  
Suzhou 215006, China

Dr. H. Q. Ta, Prof. A. Bachmatiuk, Prof. M. H. Rümmeli  
Institute for Complex Materials  
IFW Dresden  
20 Helmholtz Strasse, Dresden 01069, Germany

M. Hasan  
School of Natural Sciences  
National University of Sciences and Technology  
Islamabad 44000, Pakistan

Prof. N. M. Ahmad  
Polymer Research Lab  
School of Chemical and Material Engineering  
National University of Sciences and Technology  
Islamabad 44000, Pakistan

Prof. L. Fu  
College of Chemistry and Molecular Sciences  
Wuhan University  
Wuhan 430072, P. R. China

Prof. A. Bachmatiuk  
Polish Center for Technology Development (PORT)  
Ul. Stabłowicka 147, Wrocław 54-066, Poland

Prof. A. Bachmatiuk, Prof. M. H. Rümmeli  
Centre of Polymer and Carbon Materials  
Polish Academy of Sciences  
M. Curie-Skłodowskiej 34, Zabrze 41-819, Poland

Prof. M. H. Rümmeli  
Institute of Environmental Technology  
VŠB-Technical University of Ostrava  
17. listopadu 15, Ostrava 708 33, Czech Republic

 The ORCID identification number(s) for the author(s) of this article can be found under <https://doi.org/10.1002/admi.202000999>.

© 2020 The Authors. Published by Wiley-VCH GmbH. This is an open access article under the terms of the Creative Commons Attribution License, which permits use, distribution and reproduction in any medium, provided the original work is properly cited.

DOI: 10.1002/admi.202000999

cost-effective, long-term, high energy density, grid-scale, and portable energy generation; industrial catalysis and synthesis; as well as bio-related adaptable and wearable applications.<sup>[16–19]</sup> Compared to other approaches, such as functionalization and compositing, the chemical doping of graphene is exceptionally efficient because a small amount of dopant can significantly alter the material properties. Additionally, the doping agents can be added into the graphene lattice using conventional synthesis methods, and most synthetic doped graphenes are highly stable owing to the presence of real chemical bonds between the graphene and dopant atoms.<sup>[11,20–23]</sup>

Recently reported approaches for doping graphene include hydrothermal,<sup>[24]</sup> calcination,<sup>[25]</sup> solvothermal,<sup>[26]</sup> and ion-implantation<sup>[27]</sup> methods, as shown in Figure 1a–h. These synthetic methods have produced graphene materials with monodopants<sup>[28,29]</sup> and codopants.<sup>[30,31]</sup> Importantly,

experimentalists<sup>[32,33]</sup> and theoreticians<sup>[34]</sup> have joined forces to understand the mechanism of controlled growth with rationally designed doping features and to develop synthetic routes that are simple, economical, green, and scalable.<sup>[16,35–37]</sup> These issues are critical to the reliable and large-scale production and application of graphene derivatives.

There is considerable research on graphene doping from different aspects. In this review, we will address recent developments in doped graphene, including new synthesis routes for 2D doped graphene (single dopants, such as N, B, S, P, first three halogens, Ge, and Ga, and codopants, such as N/O), common heteroatom-induced bonding configurations, and properties of the doped graphene. Different analytical methods and more importantly the up-to-date applications enabled by intentional doping will be discussed. We hope this review would have potential interests for researchers in this field.

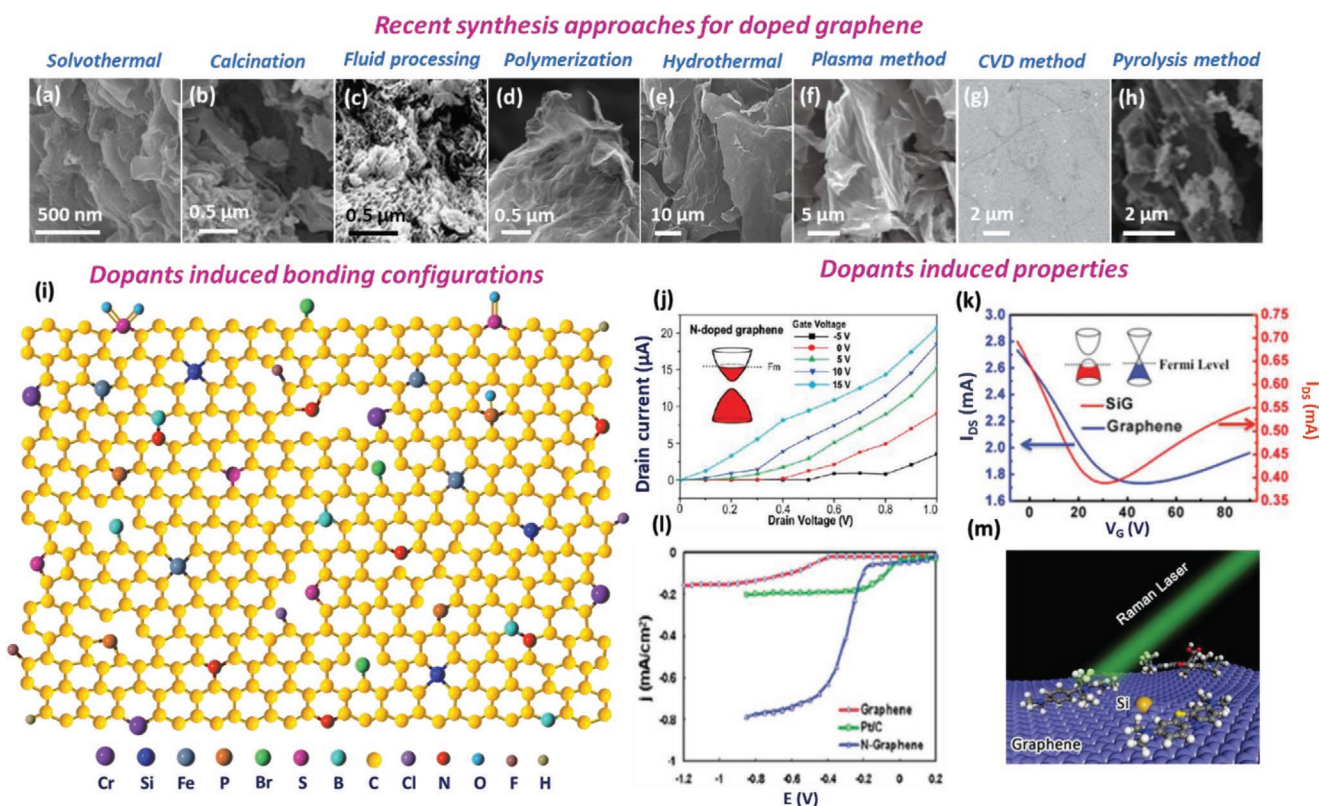


**Figure 1.** a–h) Summary of current synthetic routes developed for heteroatom-doped graphene with the corresponding example SEM micrographs. a) S-doped graphene developed by solvothermal method. Adapted with permission.<sup>[65]</sup> Copyright 2017, Elsevier. b) N/S double-doped graphene via calcination route. Adapted with permission.<sup>[25]</sup> Copyright 2016, Wiley-VCH. c) Boron heterographene by supercritical fluid processing procedure. Adapted with permission.<sup>[69]</sup> Copyright 2019, Wiley-VCH. d) Nitrogen and sulfur codoped by polymerization process. Adapted with permission.<sup>[54]</sup> Copyright 2017, Elsevier. e) N-doped graphene via hydrothermal method. Adapted with permission.<sup>[110]</sup> Copyright 2017, Elsevier. f) N & S dual doped plasma CVD method. Adapted with permission.<sup>[31]</sup> Copyright 2019, American Chemical Society. g) Bromine doped by thermal CVD route. Adapted with permission.<sup>[46]</sup> Copyright 2019, Royal Society of Chemistry. h) Phosphorous-doped graphene via pyrolysis technique. Adapted with permission.<sup>[32]</sup> Copyright 2017, American Chemical Society. i) Library of bonding configurations induced by various doping agents. j) Plot of drain current ( $I_{ds}$ ) versus drain voltage ( $V_{ds}$ ) at different gate voltages ( $V_g$ ) for nitrogen-doped graphene field effect transistors (FETs). The direct relation of  $I_{ds}$  with  $V_g$  reveals that nitrogen heterographene exhibits n-type doping effect. Adapted with permission.<sup>[60]</sup> Copyright 2009, American Chemical Society. k)  $I_{ds}$  versus  $V_{ds}$  curve. The voltage at Dirac point shifts toward the positive value, indicating p-type doping. Adapted with permission.<sup>[197]</sup> Copyright 2016, Royal Society of Chemistry. l) Voltammograms for oxygen reduction reaction (ORR) based on nitrogen-doped graphene electrode in comparison to graphitic and Pt/C based electrodes, showing the catalytic feature induced by nitrogen doping. Adapted with permission.<sup>[21]</sup> Copyright 2010, American Chemical Society. m) Schematic illustration of Si-doped graphene with three different dye probe molecules: crystal violet (CRV), rhodamine B (RhB), and methylene blue (MB), demonstrating the sensing property of heterographene. Adapted with permission.<sup>[198]</sup> Copyright 2014, Wiley-VCH.

## 2. Dopant-Induced Bonding Configurations and Properties

### 2.1. Bonding Configurations

Foreign dopant atoms can alter the properties of graphene. Hence, doping has further opened the door to many graphene-based applications including electronics<sup>[38]</sup> and sensing<sup>[39]</sup> owing to the distinct nature of each dopant.<sup>[40,41]</sup> These impurity atoms display unique bonding configurations in the graphene lattice (see Figure 1i), endowing the graphene with distinctive properties. Nitrogen typically forms three types of bonding structures: graphitic, pyridinic, and pyrrolic. The former two are planar arrangements with  $sp^2$  hybridization, while the  $sp^3$  configuration of the last one causes distortion in the planar symmetry of graphene.<sup>[42]</sup> Boron can form two planar bonding moieties that are equivalent to graphitic and pyridinic, plus one out-of-plane configuration in which the B atom sticks out from a single carbon atom.<sup>[22]</sup> Theoretically, sulfur can form several bonding arrangements, and the commonly observed configurations are the thiophenic (generating a pentagonal vacancy), and bonding similar to pyridinic and graphitic arrangements (by binding, respectively, with two and three carbon atoms). In addition, sulfur oxide structures are frequently observed.<sup>[40]</sup> Note that some foreign atoms can display the same valence but different physical arrangements: some stay in the graphene plane, whereas others are out-of-plane or even overhanging.<sup>[14]</sup> For instance, P exhibits the same three bonding forms on graphene as N (graphitic, pyridinic, and pyrrolic), however the graphitic form of P is a pyramidal overhang, whereas that of N is planar.<sup>[41,43]</sup> In the case of Si doping, an analogous overhang structure was observed, accompanied by a remarkable distortion of the planar structure of graphene. This endows Si-doped graphene with (metal-free) catalytic activity for a variety of reactions (e.g., CO oxidation). In addition, Si can establish a planar structure forming a divacancy bond with four C atoms.<sup>[44]</sup>

Halogens (F, Cl, and Br) are only one electron short of fulfilling the octet, and so they are expected to bond with one C in graphene and stick out from the basal plane.<sup>[41]</sup> Such a configuration would change the hybridization of carbon from planar  $sp^2$  to trigonal planar  $sp^3$ , thereby introducing curvature into the graphene sheets. This effect is especially pronounced for bromine due to its large size.<sup>[45–48]</sup> On the other hand, the smaller F tends to fully cover the graphene sheet to form fluorographene (CF)<sub>n</sub>. Unlike other types of halographene, this is the only stable form for fluorine doping, and (CF)<sub>n</sub> acts as an insulator by restricting the delocalized electrons.<sup>[41,49]</sup>

Metals displaying different bonding states with graphene have also been reported, such as Fe and Cr.<sup>[50,51]</sup> Analogous to Si, Fe forms a divacancy planar or out-of-plane graphitic bonding system. Cr has demonstrated pyridinic and pyrrolic configurations, but the disruption caused by its doping is stronger (viz., the structural distortion is greater) because of the large size.<sup>[52,53]</sup> One thing to bear in mind is that the graphitic bonding configurations are generally more stable than others, especially for smaller dopant atoms. The reason is likely because of the preservation of the graphitic hexagonal lattice which is stable.<sup>[41]</sup>

In addition to the commonly bonding configurations derived theoretically or observed experimentally for chemical dopants,

other bonding arrangements are also possible, and they can be interesting in many ways. Currently, codoped heterographene has drawn considerable interest.<sup>[54,55]</sup> The goal of codoping is to create superior synergy by joint contributions to a particular property.<sup>[27]</sup> For instance, P/N codoping is useful for designing improved n-type effect, which is not seen in the individually doped materials. As another example, when B and N atoms are doped alone in graphene, they tend to assume a scattered and random distribution. However, when doped together they preferentially form B-N bonds and even hexagonal patches (h-BN) in pristine graphene system.<sup>[56,57]</sup> These integrated B-N bonds cancel out the doping effect, and the material behaves more like pristine graphene.

### 2.2. Properties Provided by Doping Agents

Owing to their valence electronic configurations and atomic size (especially for bulky atoms, such as S and Br), dopants cause two major transformations: destruction of the pristine graphene's hexagonal symmetry, and alteration of the electronic structure. These changes in turn influence the properties of the doped graphene such as the bandgap ( $E_g$ ), magnetic moment, thermal stability, electron mobility, spin densities, reactivity, optical characteristics, and photoresponses.<sup>[11,41,58]</sup> Some of the typical properties induced by dopants are summarized in Figure 1j–m. Depending on the type of dopant(s), bonding configuration, and the degree of doping, new or improved properties may arise that are advantageous for particular applications. The ability to customize graphene properties by heteroatom doping is vital for the design and discovery of novel characteristics in graphene materials and further extension of their exploitations.

The lattice parameters of graphene are slightly altered upon doping. For example, the B–C bond length is greater than the C–C bond ( $\approx 1.5$  and  $1.41 \pm 0.01$ , respectively). Some dopants present n-type doping (N in the graphitic state, P, Ga, Fe, etc.)<sup>[50,59–61]</sup> while others display p-type effect accompanied with a downshift of the Fermi level toward the Dirac point (e.g., N in the pyridinic state, B, S, Si, O, and halogens).<sup>[46,62–64]</sup> It is generally thought that the opening of the bandgap is due to symmetry breaking induced by the doping atoms. Therefore, the bandgap ( $E_g$ ) is usually a function of the doping level.<sup>[41]</sup> S-doped graphene has a high catalytic activity (e.g., for the oxygen reduction reaction, ORR), because of a valence orbital mismatch to carbon despite their comparable electron affinities ( $\approx 2.58$ ).<sup>[65]</sup> Meanwhile, metal doping endows graphene with single-atom catalytic features, as pointed out by Ta et al. for chromium doping.<sup>[66]</sup> Importantly, different bonding configurations of the same dopant can introduce distinct properties. Graphitic N is conductive,<sup>[59]</sup> while pyridinic N is attractive for storage purposes (particularly, high energy capacity in batteries).<sup>[67]</sup> N-doped graphene is promising in spintronics because of its magnetic properties. Specifically, pyrrolic and pyridinic N-doped graphene both have nonbonding electrons, the former displays strong magnetic properties and the latter displays poor ones. Compared to N, P as a doping impurity causes a stronger magnetic effect.<sup>[11,41]</sup> Moreover, since P has a lower electron affinity than carbon (2.11 vs 2.55), the electron density in the C–P bond shifts more toward carbon as compared to the C–N system, where the electron density shifts toward N. As mentioned

earlier, halogens (F, Cl, and Br) tend to be covalently doped into graphene and transform the  $sp^2$  carbon into  $sp^3$  hybridization (tetrahedral symmetry). Iodine, however, tends to form a charge transfer complex (ionic bond) rather than covalent bond with graphene, and this leaves the  $sp^2$  symmetry intact. Previous studies demonstrated that graphene doped with F and Cl are direct bandgap semiconductors, whereas brominated graphene is an indirect bandgap semiconductor.<sup>[49,68]</sup> Additionally, smaller dopant atoms (such as B and N) induce less structural deformation, while bigger atoms (such as Br, S, and Fe) promote larger structural defects. These transformations may be deliberately utilized to modify graphene.<sup>[22,40,69]</sup> In the case of codoping, B/N is of special interest. Graphene, with h-BN patches, behaves like pristine graphene, because B and N have opposing effects—N creates conducting electrons, while B create holes upon doping into graphene. Furthermore, B/N codoped graphene is thermally less stable than N-doped graphene but more stable than B-doped graphene. Unlike the B/N system, other codoped atoms, such as N/S and N/P tend to be distributed randomly in the material. On the other hand, one of the doped species may favor a particular bonding configuration in the presence of another specific dopant. For example, P and S promote pyridinic and graphitic nitrogen configurations, respectively.<sup>[41]</sup> It is worth noting that, when one of the codopants is strong (i.e., more tightly bound with carbon, such as nitrogen) and another is weak (especially heavy atoms like aluminum), the codoping system is more robust than doping with a single weak dopant.

An example is the N/Al codoping structure, which is more stable than the Al-doped structure<sup>[70–72]</sup> because of a reduced formation energy in the codoped system.<sup>[73]</sup>

### 3. Analytical Approaches

To exploit the potential of graphene doping to the maximum, it is critical to understand the different attributes of doped graphene in detail, such as the topography, morphology, quality, number of layers, and the doping system (such as doping chemical state, doping level, and distribution), because these characteristics strongly impact the material's properties.<sup>[41,69,74]</sup> Thus, various spectroscopic and microscopic techniques have been used to comprehensively examine the chemical derivatives of graphene, and some of them are reviewed below.

Raman analysis is an efficient and simple spectroscopic technique for inspecting the structural features (e.g., number of graphene layers, layer stacking order, structural disorders, details about the quality and crystallinity, and evidence of doping).<sup>[60,75,76]</sup> The intensity ratio of the 2D and G peaks ( $I_{2D}/I_G$ ) is generally used to estimate the number of layers.<sup>[77]</sup> For monolayer graphene, the 2D peak is narrow and symmetric in shape, with a higher intensity than that of the G mode. In single layer graphene,  $I_{2D}/I_G$  is often around  $\geq 1.5$  (without being rigorous), and this ratio decreases with additional layers<sup>[78–80]</sup> as shown in Figure 2a. The full width at half maximum (FWHM)

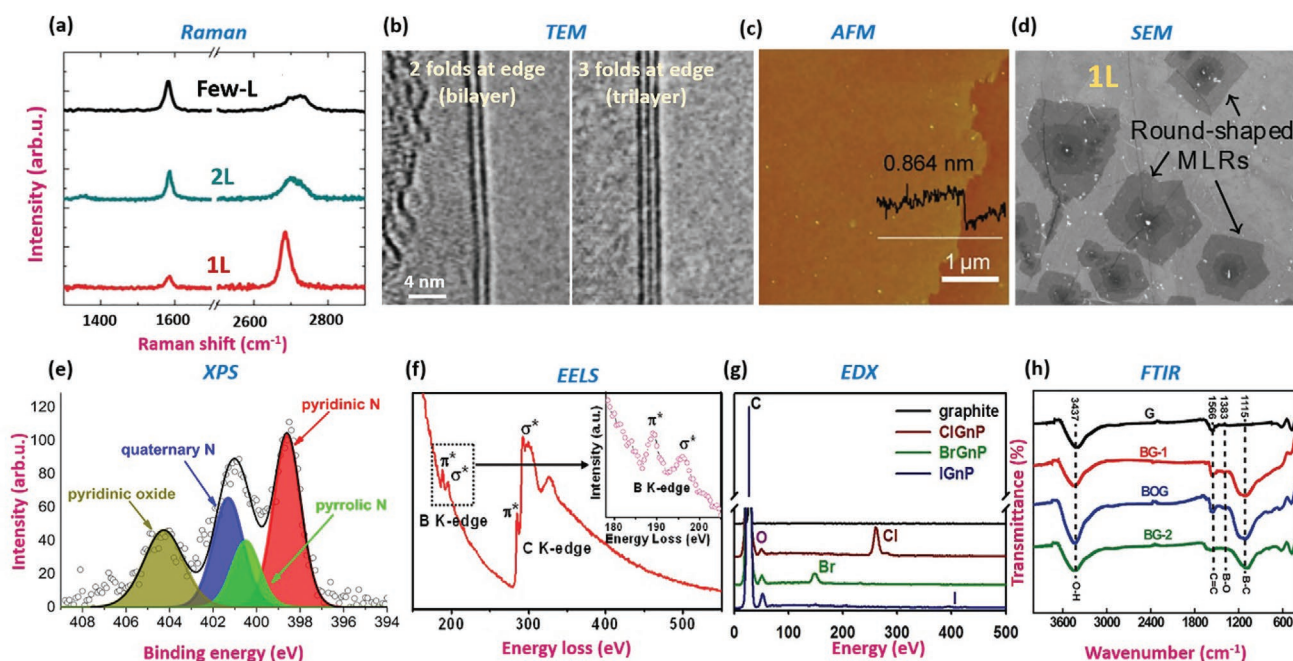


**Figure 2.** a) Raman spectra of pristine graphene with different thicknesses. 1L (pristine graphene), 2L, and few-L stand for mono-, bi-, few-layers of graphene, respectively. Adapted with permission.<sup>[79]</sup> Copyright 2010, Springer Nature. b) TEM micrograph of double and trilayer boron/nitrogen dual-doped graphene. Adapted with permission.<sup>[57]</sup> Copyright 2010, Springer Nature. c) AFM image of single layer B-doped graphene. Adapted with permission.<sup>[88]</sup> Copyright 2013, Wiley-VCH. d) SEM image showing the various thicknesses in graphene (1L: single layer, MLRs: multilayer graphene regions). Adapted with permission.<sup>[199]</sup> Copyright 2017, Elsevier. e) Broadview XPS spectrum of N 1s and the different states. Adapted under the terms of the Creative Commons Attribution 4.0 License.<sup>[42]</sup> Copyright 2018, The Authors, published by Springer Nature. f) EELS spectrum of B-doped graphene. Inset: magnified view of the dashed square region. Adapted with permission.<sup>[13]</sup> Copyright 2012, American Chemical Society. g) EDS results of pristine and halogenated graphene (Cl, Br, and I). Adapted with permission.<sup>[92]</sup> Copyright 2013, Springer Nature. h) FTIR spectra of different samples of B-doped graphene. Adapted with permission.<sup>[94]</sup> Copyright 2018, Elsevier.

of the 2D peak also reflects the number of layers. Monolayer graphene often has a FWHM value below  $40\text{ cm}^{-1}$  (again, this value is changeable).<sup>[46,81]</sup> Raman mapping can be used to evaluate the uniformity and homogeneity of graphene thickness, as well as the distribution of defects and/or doping within the measured sample region.<sup>[82]</sup> Moreover, Raman analysis helps confirm doping by the emergence of D (which might originate from either intentional doping or other structural disorders) and D' shoulder peaks near the G mode. The position, shape, and shift of Raman peaks can also provide information about the doping and the number of graphene layers.<sup>[38]</sup> A blueshift and/or relative reduction in intensity of the 2D peak with respect to pristine graphene can be attributed to the doping and an enhanced number of layers, respectively.<sup>[12,46,77]</sup>

In contrast, transmission electron microscopy (TEM) can precisely identify the number of graphene layers by counting the folds at the graphene edge in micrographs (Figure 2b), which is also backed by fast Fourier transform of the micrograph.<sup>[33,83]</sup> High-resolution TEM (HRTEM) can assess the material quality and crystalline hexagonal symmetry with atomic resolution.<sup>[57,84,85]</sup> In addition, selective area electron diffraction (SAED) analysis is useful for determining the lattice parameters, crystal orientation, stacking order, number of graphene layers, and more importantly the sample crystallinity over a small region. A single set of hexagonal spots obtained from the sample suggests better crystal symmetry, whereas continuous circles or diffuse spots indicate an amorphous region.<sup>[86]</sup> The atomic force microscopy (AFM) technique can reveal accurate details about the sample topography, such as film continuity, cracks, wrinkles, folds, smoothness, and contaminants on the surface.<sup>[87,88]</sup> AFM provides 3D imaging of the surface up to the nanoscale, and the number of graphene layers can be determined from the height profile. The commonly reported AFM intensity profile height for single layer graphene is  $<1\text{ nm}$  (Figure 2c), and the height increases when there are more layers.<sup>[13]</sup> Both conductive and nonconductive surfaces can be measured by this technique. Similar to AFM, scanning electron microscopy (SEM) uses an incident/primary electron beam to strike the sample, creating secondary electrons and several other signals that provide different types of information. By creating a 3D micrograph of the sample, SEM can be a supportive characterization technique for graphitic materials at low resolution and large areas, primarily providing the topographical and morphological information (such as, grain shape, grain boundaries, patches, contaminations, and number of layers). This technique is also applicable to both conductive and nonconductive surfaces: the former is measured directly, while the latter needs special treatment such as gold coating (Figure 2d).<sup>[75,89]</sup>

Various aspects of heterodoped graphene can be evaluated, such as the doping agent/s-induced bonding configurations, degree of doping, and elemental distribution/s. Several techniques exist to measure these characteristics, with pros and cons for each. X-ray photoelectron spectroscopy (XPS) uses X-rays to eject core level electrons, whose binding energy is specific to the elemental atom and the bonding state. It is a sensitive way to measure the surface doping configurations, oxidation states, as well as the amount of doping agent present (Figure 2e). Electron energy loss spectroscopy (EELS), which is integrated with TEM and scanning TEM (STEM), is based on the kinetic energy loss

of electrons upon inelastic collision with atoms in the sample. EELS is also sensitive to the chemical composition, bonding configuration, and electronic structure in thin samples because of its transmission-based mechanism. Thus, it is usually considered the best tool for establishing the chemical identities and bonding at the atomic level (Figure 2f).<sup>[15,90,91]</sup> Moreover, EELS mapping can reveal the elemental distribution even at trace amounts.<sup>[13]</sup> For analysis of the chemical composition inside the sample to a depth of a few micrometers and mapping the elements over a broader region, the energy dispersive X-ray (EDS) technique can be used, which measures the characteristic X-ray emitted by each atom in the sample under an electron beam. EDS can be integrated with both SEM and TEM (see Figure 2g).<sup>[92]</sup> On the other hand, unlike XPS and EELS, EDS is not appropriate for detecting the bonding states.<sup>[93]</sup> Another sensitive, simple, fast, and universal analytical approach is Fourier transform infrared (FTIR) analysis, which is able to recognize chemical bonds, chemical reactions, contamination in the specimens, and even chemical structure of the analyte (Figure 2h).<sup>[94,95]</sup> FTIR is, however, unsuitable for detecting monoatomic moieties (e.g.,  $\text{H}^*$  radical or  $\text{Na}^+$  ion), homoatomic molecules (e.g.,  $\text{N}_2$  and  $\text{Cl}_2$ ), and the chemical states, as compared to XPS and EELS. Besides those mentioned above, many other analytical methods could be exploited for various purposes. Overall, careful characterization helps to reveal the growth mechanism and screen for desired characteristics in the materials, thus contributing to the development of scale-up practical applications.

More significantly, the joint use of atomic resolution microscopy and spectroscopy has made it possible to directly spot impurity atoms in the graphene lattice together with their precise chemical nature, even in the presence of camouflage contaminations. A usual problem with heteroatom-doped graphene structures is contamination comprised of carbon-based structures, whose bonding environment is analogous to that expected for atomic dopants inside the graphene lattice (Figure 3a,b).<sup>[15]</sup> Even detecting the atomic bonding environment is not enough to resolve this, as the contaminant atoms can easily be mistaken for doping agents. In most cases, successful doping is evaluated indirectly from nonlocal spectroscopic signatures, e.g., by comparing XPS data with existing literature. This was reported by Susi et al. for phosphorous-implanted graphene, where silicon impurities cause identical signals.<sup>[96]</sup> Since the contamination hinders adequate assessment of heterographene as well as reducing the sample quality, advanced atomic-scale characterization methods would provide significant in-depth insight into heterographene and its application in various devices. For instance, scanning tunneling microscopy is a powerful tool for local characterization.<sup>[97]</sup> Although lacking direct chemical sensitivity, it has been used to confirm the local bonding of light impurities (e.g., N and B) in graphene. Recent advances in aberration corrected STEM have similarly enabled the direct visualization of individual atoms in low-dimensional heterographene materials.<sup>[98]</sup> When atomic resolution STEM is used for EELS, even the precise nature of atomic bonding can now be resolved. For instance, researchers have directly observed nitrogen and oxygen atoms in N-doped graphene lattice and graphene oxide, respectively, along with their chemical forms via atomic resolution imaging (Figure 3c,d).<sup>[99]</sup> (Surprisingly, oxygen bound with three carbon atoms was also visualized, which had been rarely

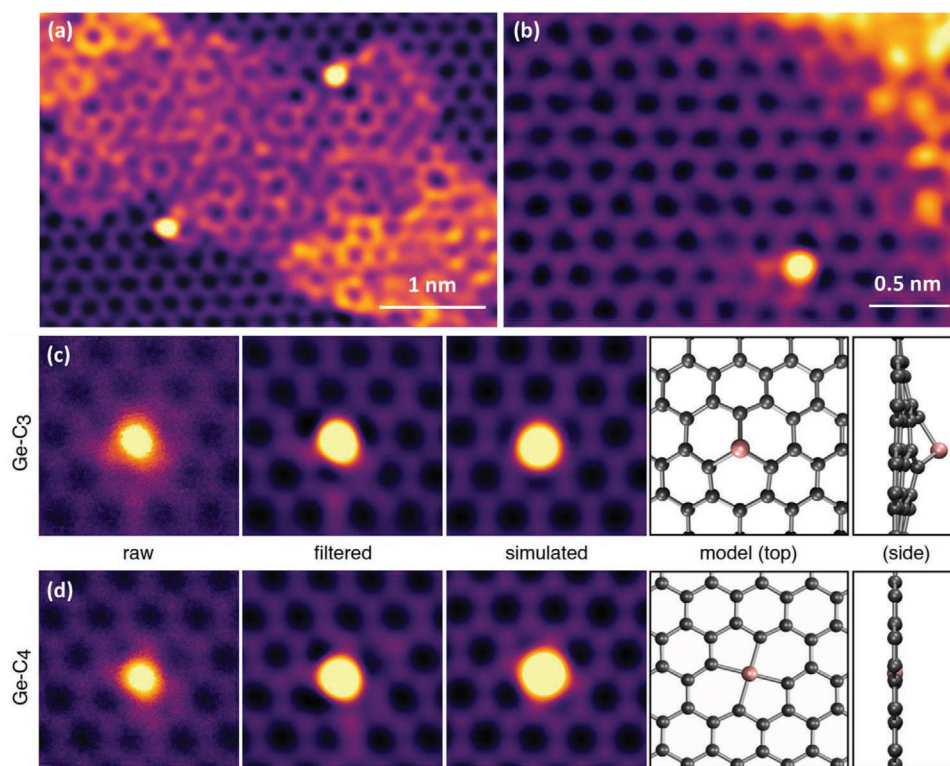


**Figure 3.** a,b) Two and one Ge atoms (bright spots) bound to graphitized contaminations and graphene lattice, respectively. c,d) Atomic resolution STEM image, the corresponding filtered and simulated images, and model structures of Ge implanted in graphene and bound by three and four carbon atoms, respectively. These images suggest the potential of atomic resolution STEM for the direct observation of doping atoms along with the bonding configurations in graphene, as well as the ability to distinguish dopant in the graphene lattice from that in graphitized contaminations. Adapted with permission.<sup>[15]</sup> Copyright 2018, American Chemical Society.

reported before.) In addition to that, EELS can provide adequate electronic structural information down to the single atom scale, as presented by Kepaptsoglou et al. for boron-implanted graphene.<sup>[44,100]</sup> Finally, thanks to recent progresses in electron beam manipulation, it is possible to controllably create and heal defects in graphene and to move them.<sup>[98,101–103]</sup> This concept was presented by Tripathi et al. (who attempted to displace Ge atoms in graphene lattice) and other researchers.<sup>[15,66,104,105]</sup> Atomic resolution study has further advanced noncarbon elemental doping of graphene (either singly or as a codopant), which is important for understanding the novel attributes of heterographene and developing related applications.

## 4. Synthesis

### 4.1. N-Doped Graphene

Because of its comparable atomic size with carbon and greater electron affinity (3.04), nitrogen is highly suited to substitute carbon in graphene without causing serious structural effects.<sup>[40,41]</sup> As a result, it is the most comprehensively investigated dopant from both theoretical<sup>[14,106]</sup> and experimental perspectives. The reported synthetic methodologies range from chemical vapor deposition (CVD)<sup>[33,107]</sup> to hydrothermal<sup>[108–111]</sup> and ion implantation<sup>[112]</sup> methods. Different synthesis parameters can be adjusted to tailor the N-doped graphene, e.g., the

number of layers, quality, doping content, and doping configurations. Recently, Jia et al. produced continuous single layer N-doped graphene by the CVD approach at several growth temperatures (230–600 °C), as illustrated in **Figure 4a**. This approach uses a single solid precursor (pentachloropyridine) that simultaneously supplies both carbon and nitrogen. When there are two or more precursors, the mechanism for controlled growth becomes complicated due to the different properties of carbon and doping agent, such as the thermal properties, decomposition rate, and chemical compatibility of decomposed moieties with each other as well as with the growth substrate. In contrast, a sole precursor containing both carbon and doping elements can simultaneously introduce the different chemical species in a controlled manner for the large-scale growth of uniform and high-quality doped graphene.<sup>[88]</sup> Jia et al. found that the quality of the grown material is degraded when raising the growth temperature, as can be observed in **Figure 4b–f**. The proposed reason is that the chlorine radical drastically etches the copper surface, and the resultant coarse surface is not conducive to the deposition of high-quality graphene. They also showed that the growth temperature can be used to produce single layer N-doped graphene (**Figure 4g,h**) with a particular doping configuration. For instance, dominant graphitic and pyrrolic N-doped graphene was grown at low (230–300 °C) and at high (400–600 °C) temperatures, respectively.<sup>[38]</sup> Similarly, another group conducted CVD at ambient pressure using gaseous precursors (ammonia as the N source and methane as the C source), and reported

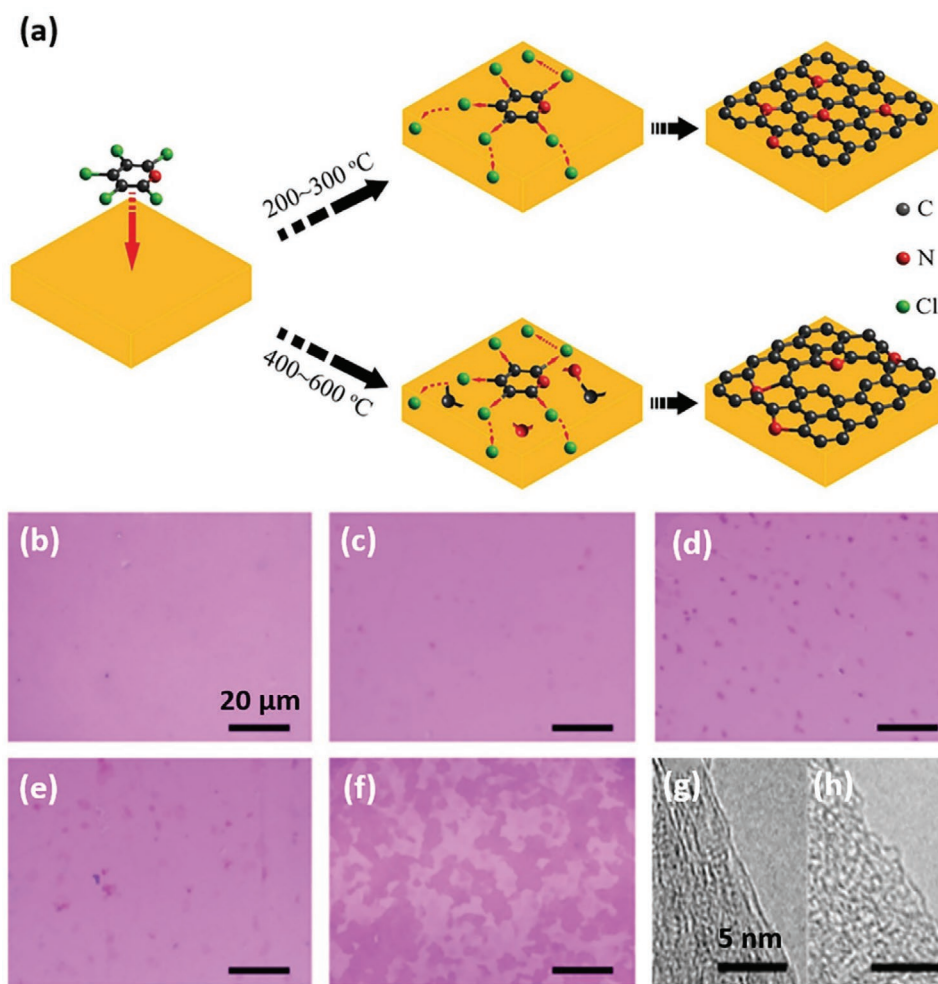


**Figure 4.** a) Growth schematic of N-doped graphene at different temperatures. A low temperature (230–300 °C) leads to dominant graphitic nitrogen doping, while a high temperature (400–600 °C) mainly results in pyrrolic N-doping. b–f) The corresponding optical images over silicon substrates. g, h) HRTEM micrographs of monolayer N-doped graphene grown at 300 and 500 °C, respectively. Adapted under the terms of the Creative Commons Attribution 4.0 License.<sup>[38]</sup> Copyright 2016, The Authors, published by Springer Nature.

that the growth temperature as well as growth time could be exploited for controlled N doping.<sup>[33]</sup> Maddi et al. implemented a laser-assisted strategy, by depositing a Ni thin film (60 nm) onto a SiO<sub>2</sub> substrate followed by the deposition of an amorphous carbon nitride thin film (a-C:N, 10 nm). Afterward, the a-C: N/Ni/SiO<sub>2</sub> hybrid film was thermally treated to grow N-doped graphene. The prepared sample consisted of a few layers with dominant pyridinic doping structure, as can be viewed in Figure 2e. The doping content (2–3 at%) was shown to be reproducible and stable, being independent of the N concentration in the a-C: N film.<sup>[42]</sup> While N-doped graphene with minor defects are not common, it was produced by Sarau et al. via ex situ doping of pristine graphene. In this two-step method, CVD-grown pristine graphene was treated with NH<sub>3</sub> after transfer to a sapphire substrate. According to the Raman study, the produced samples were predominantly monolayers. XPS analysis revealed the coexistence of pyrrolic and dominant pyridinic states (11 at% in total). This study points out that graphene doping can be achieved without causing significant defects following an ex situ route.<sup>[107]</sup>

Ion implantation is another important and mature technique for achieving adequate graphene doping, and it has shown great promise.<sup>[112–114]</sup> One research team had proposed that heteroatoms can be successfully incorporated in the graphene lattice by ion irradiation under the following conditions: i) the energy of incident ion should be enough to knock out the carbon(s); ii) kinetic energy remaining in the ion after collision with carbon lattice should be small enough to allow it to be lodged in the graphene lattice; and iii) the implanted ion should form covalent bond with atoms of the vacancy to reach a stable configuration.<sup>[15]</sup> However, contradicting the above conditions, Bai et al. found that the ion incident angle is more important than ion energy for the productivity and quality of doping. Particularly, compared to the perpendicular direction, ion bombardment tilted at an angle to the normal is more favorable. At the optimal angle of 70°, the productivity was boosted by more than 25%, together with enhanced quality of substitution.<sup>[27]</sup> This observation could lead to a deeper insight about the ion implantation mechanism that is useful for realizing controlled doping. Zhao et al. used such a method to obtain single-layer nitrogen-implanted graphene

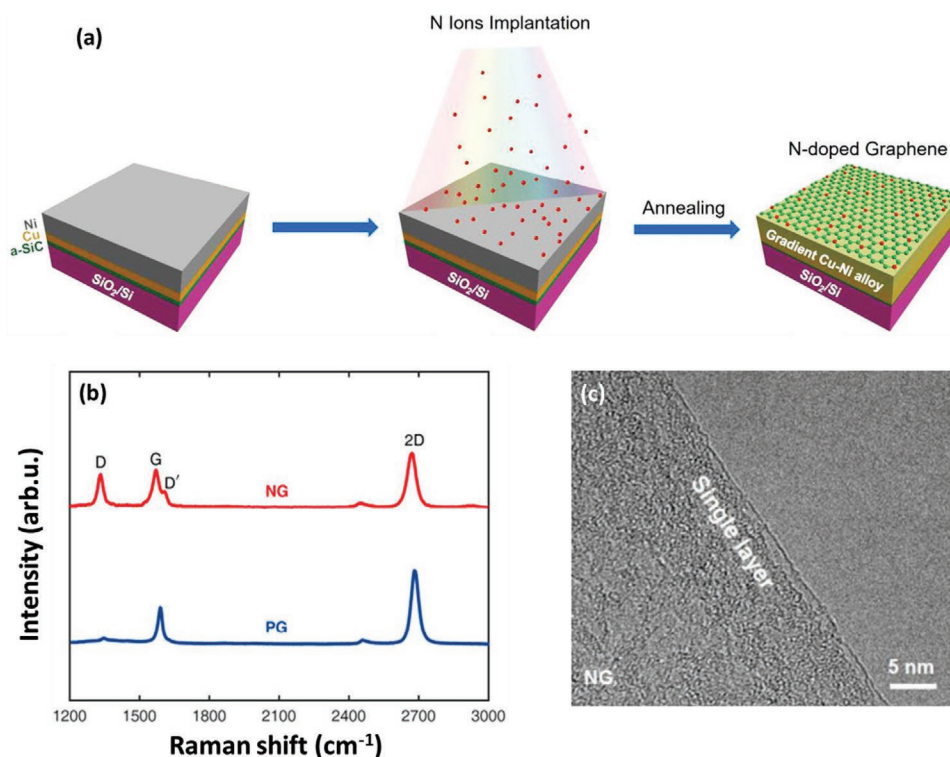


**Figure 5.** Schematic illustration of ion implantation growth method for nitrogen heterographene (NG). b) Corresponding Raman spectra of pristine (PG) and nitrogen-doped graphene. c) HRTEM micrograph of monolayer NG. Adapted with permission.<sup>[115]</sup> Copyright 2018, Elsevier.

with improved quality (Figure 5a–c). Notably, they used a multi-layer substrate (Ni/Cu/amorphous-SiC/SiO<sub>2</sub>/Si) in which amorphous-SiC provided carbon feedstock, and control over nitrogen content was achieved by monitoring the N ion fluence.<sup>[115]</sup> The advantages of this method are the compatibility with microelectronic industry and the feasibility for even heavy atomic dopants (e.g., germanium).<sup>[15,115,116]</sup> Scardamaglia and his colleagues came up with a similar implanting method. Unlike Zhao et al., these authors employed a two-step approach of CVD growth of graphene followed by nitrogen ion treatment (ion implantation), achieving a high nitrogen content ( $\approx 8$  at%) without formation of graphene lattice defects. Furthermore, thermal annealing was used to tune the doping configuration, such as converting pyridinic to graphitic nitrogen. This investigation suggests that the ion implantation method can achieve a high doping content as well as thermal interconversion among different bonding configurations. It will facilitate the understanding of distinctive properties of foreign atoms in a specific bonding form and relate them to the corresponding applications.<sup>[64]</sup> Recently, Hofer et al. demonstrated nitrogen doping by irradiating nitrogen ions onto graphene on a TEM grid, and atomic resolution imaging confirmed that the doped nitrogen prefers to bind with three carbon atoms (graphitic form).<sup>[99]</sup> Based on these observations from different research groups, high-quality tunable nitrogen doping of graphene is possible; and particular bonding configurations, a large continuous area, and single-layer thickness can be achieved by controlling the synthesis parameters such as, the growth temperature, growth duration, precursor sublimation temperature (for solid precursors only), and even by laser deposition and ion implantation methods.

#### 4.2. Boron-Doped Graphene

Similar to nitrogen, B-doped graphene has been reported with different numbers of layers, doping content, and bonding configurations. The synthetic approaches include pyrolysis<sup>[117]</sup> and hydrothermal methods.<sup>[24,118]</sup> Wu et al. used novel precursors (9,10-dimesityl-9,10-diboranthracene (DBA(Mes)<sub>2</sub>) as the boron source and toluene as the carbon source) to customize the quality of B-doped graphene using a bubbler-assisted CVD method. The resultant sample was of high quality and consisted of single layers with a significant B content up to 4.6 at%.<sup>[119]</sup> Solid precursors are generally preferred as the growth feedstock due to the large range of choices, their benign property, stability, and ease of handling.<sup>[120]</sup> Srivastava and colleagues used B powder as the boron source and liquid ethanol as the carbon source to produce B-doped graphene by low pressure CVD. The as-grown sample was few-layered according to Raman analysis, whereas the XPS result revealed two dominant bonding configurations (BC<sub>3</sub> (graphitic form) and BC<sub>4</sub>) with a doping concentration up to 4.9 at%.<sup>[39]</sup> Incorporation of boron into the graphene framework has also been achieved via a two-step CVD procedure. Pristine graphene is deposited by CVD, transferred to a target substrate, and then treated with a boron source solution. XPS analysis verified the presence of boron, and Raman mapping concluded that the as-grown sample was comprised of double layers on average.<sup>[81]</sup> Additionally, the novel route developed by Bleu and collaborators used a solid precursor to control the doping concentration. They used a laser deposition method identical to that for nitrogen doping (already described in Section 4.1,<sup>[42]</sup>). The growth schematic is depicted in Figure 6a.

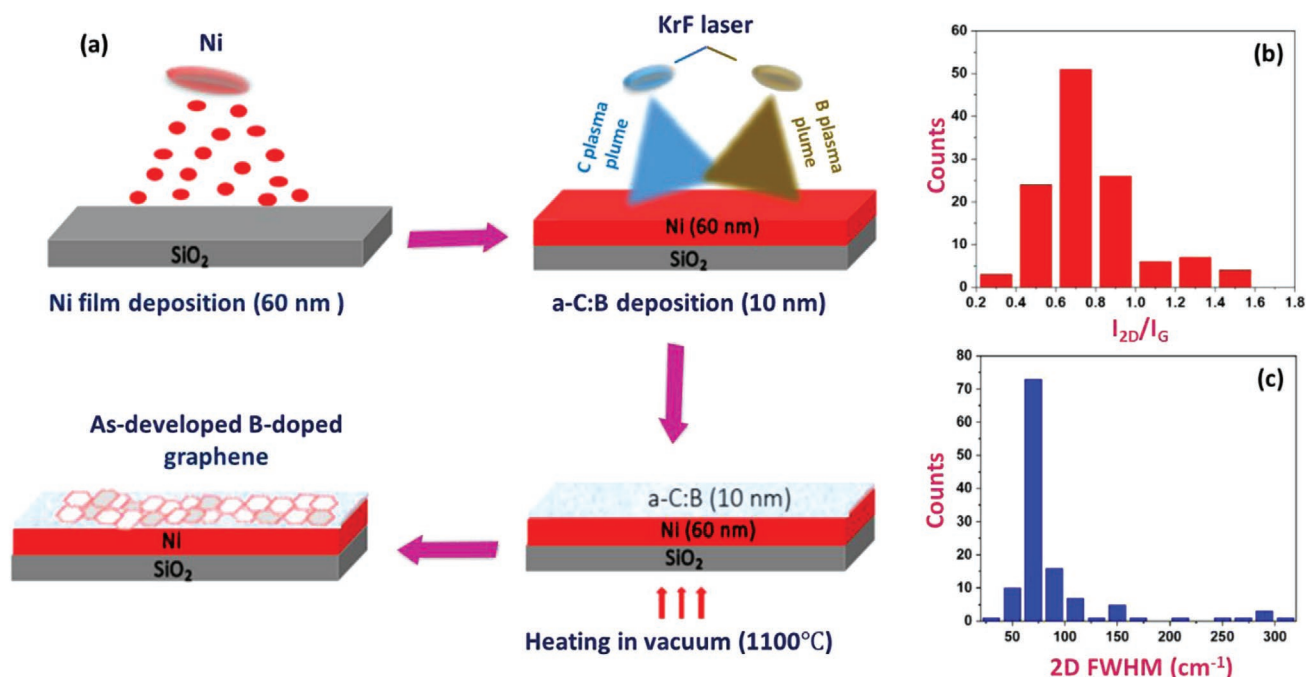


**Figure 6.** a) Schematic illustration of B-doped graphene synthesis by pulse laser codeposition method. b,c) Histograms for the intensity ratio between the 2D and G peaks ( $I_{2D}/I_G$ ) and the 2D peak width (FWHM), respectively. Both histograms indicate few-layer B-doped graphene. Adapted with permission.<sup>[121]</sup> Copyright 2020, Elsevier.

In the as-prepared sample, up to 2 at% of boron was distributed in few layered graphene as demonstrated in Figure 6b,c.<sup>[121]</sup> This study demonstrates the versatility of the laser deposition route, which could be extended beyond boron and nitrogen doping. Dianat et al. reported an economical and simple way to integrate boron into graphene. In their ex situ doping approach, pristine monolayer graphene was grown by CVD and transferred to a silicon substrate predoped with boron. Finally, the substrate was heated at 400 K to allow boron integration into graphene. This route using a relatively low temperature may be applied to many other types of heterodoping.<sup>[122]</sup> In addition, argon flow can be used to control the growth, as recently established by Boukhvalov et al. in a bubbler-assisted CVD procedure. Argon (as the buffer gas) at different flow rates (50 and 100 sccm) was passed through the bubbler containing boron source. In general, different parameters in CVD can be optimized for tunable growth.<sup>[123]</sup> Romani et al. used a single liquid precursor (isopropyl borate) and cracked it to grow B-doped graphene by the CVD route. At the optimal growth temperature (1000 °C), pressure (75 mTorr), and growth duration (5 min), single layer B-doped graphene can be achieved, and the presence of doping was shown by XPS and Raman analyses.<sup>[124]</sup> Significantly, this study demonstrates the usefulness of a single liquid precursor, whereas single solid precursors are commonly reported.<sup>[88]</sup>

### 4.3. Sulfur-Doped Graphene

Sulfur is a bulky dopant, and its low electronegativity means that it does not bind very strongly with graphitic carbon.<sup>[40]</sup> Among numerous recent studies, Guo et al. employed a two-step CVD technique to grow S-doped graphene with excellent quality. First,

pristine graphene was deposited via CVD and transferred to a substrate mediated by polymethyl methacrylate (PMMA). The graphene was then once again subjected to CVD in the presence of H<sub>2</sub>S as the S source under medium heating (500 °C). The goal was to preserve the quality of the grown film by limiting the number of transfer steps to one. The high quality of the product was confirmed by both SAED and Raman studies.<sup>[86]</sup> This study shows that, in addition to optimized synthesis parameters, the number of transfer steps should be reduced to ensure excellent quality and crystallinity in the doped graphene.

### 4.4. Phosphorous-Doped Graphene

Generally, preparing phosphorous-doped graphene is considered challenging because the large size of P hinders its incorporation into the graphene system. This is why the growth of such materials is rarely reported as compared to other dopants, such as nitrogen and boron.<sup>[11,40,125]</sup> However, we have already mentioned that ion implantation method is adequate for inserting large atoms into graphene. He et al. successfully implanted phosphorous into graphene with minimal defects. First, they employed a gold coating on CVD graphene as protection layer against damage by the high-energy ions. Second, a subsequent posthealing step further restored the structural integrity of heterographene. The authors claimed a record phosphorous doping content of 4.22 at%.<sup>[126]</sup> It is challenging to correctly identify the dopants because of the identical signal produced by contaminations. Significantly, Susi et al. effectively addressed this issue for phosphorous-doped graphene developed by the ion implantation route. They used atomic resolution imaging along with EELS to precisely confirm the integration of

phosphorous into graphene with a pyramidal overhang bonding configuration.<sup>[96]</sup> This approach also demonstrates the advancement of inspection techniques down to the atomic scale.

#### 4.5. Metal-Doped Graphene

Metal-doped graphene materials are rarely reported, despite their unique potential applications, such as single atom-promoted catalysis. This is probably due to the low binding energy of metals with graphene, which sometimes makes it hard to overcome the cohesive force between the metal atoms. As a result, the metal tends to form clusters.<sup>[41]</sup> Among the limited reports, iron-doped graphene was prepared by a two-step CVD method. The corresponding chromium ex situ doping of graphene was presented by Ta et al., and their HRTEM study revealed that chromium can be utilized as a catalyst for the growth of graphitic materials.<sup>[53,66,127]</sup> While gallium doping in the real world is not common either, Mach et al. produced Ga-doped graphene using a two-step CVD method. Pristine graphene was grown on copper foil and subsequently transferred to a silicon substrate. Afterward, it was subjected to thermally produced Ga vapors in an ultrahigh vacuum to introduce Ga into graphene. Notably, Ga doping up to a certain concentration was found to enhance the n-type behavior but adding more Ga had the opposite effect. This phenomenon can be explained theoretically as follows. At low doping levels, the Ga-graphene interaction (adhesive bond) is dominant; while at higher doping level, the Ga–Ga interaction becomes more prominent, and so Ga clusters are formed and inhibit the n-type behavior.<sup>[41,50]</sup>

#### 4.6. Germanium-Doped Graphene

One advantage of ion implantation over other synthesis techniques is the ability to insert heavy atoms (e.g., Ge) into the graphene lattice.<sup>[41,114]</sup> For instance, Tripathi and teammates recently realized germanium doping in graphene by a low-energy ion implantation method. The atomic resolution assessment (direct observation for impurities) revealed a pyramidal out-of-plane bonding configuration with monovacancy (Ge–C<sub>3</sub>). This study demonstrated that ion implantation can be carried out at an energy below the displacement threshold for graphene, which can be extended to the controllable doping of other low-dimensional materials.<sup>[15]</sup>

#### 4.7. Halogen-Doped Graphene

Early on, we mentioned that F, Cl, and Br could be incorporated into graphene with covalent bonding. This may explain why these three halogens are reported in the literature as true chemical doping, while iodine generally prefers ionic doping by forming a charge transfer complex.<sup>[49,78,128,129]</sup>

##### 4.7.1. Fluorine Doping

Kováříček et al. reported a two-step CVD route for F-doped graphene. Pristine monolayer graphene was deposited by

conventional cracking of a gaseous precursor (methane) and transferred to a silicon substrate. Then, it was treated with the vapors from a solid fluorine precursor (XeF<sub>2</sub>) for doping. This method was able to achieve a high fluorine doping level (up to 10 at%). As discussed in Section 2.1, F forms single covalent bond with graphene with a high C–F binding energy of 688.2 eV. Such a bonding state favors the conversion of sp<sup>2</sup> carbon to sp<sup>3</sup>. Interestingly, the Kováříček group found the fluorinated graphene to be a useful intermediate for further synthesis, such as the grafting of thiol group.<sup>[130]</sup> Similarly, in another two-step CVD strategy, pure graphene is exposed to CF<sub>4</sub> plasma as the F source at room temperature. XPS analysis revealed both ionic and covalent states of fluorine with the respective binding energies of 686.7 and 688.9 eV. The coexistence of two states for fluorine is attributed to the extremely strong electron affinity of fluorine (3.98).<sup>[131]</sup>

##### 4.7.2. Chlorine Doping

Cl-doped graphene has been synthesized using a few schemes.<sup>[132]</sup> Nevertheless, Copetti et al. developed a two-step photochlorination method, in which pristine graphene is pregrown elsewhere (commercially available CVD-grown graphene on silicon was used in this case) and then exposed to Cl<sub>2</sub> gas under ultraviolet radiation. The doping mainly occurs at the edges and defects of the graphene (Cl/C ratio ≈ 0.1). Notably, the doped Cl is sensitive to the laser irradiation used during material characterization. Such a laser-based technique allows one to tune the doping level at the nanoscale, which can lead to interesting applications.<sup>[133]</sup>

##### 4.7.3. Bromine Doping

Since the bromine atom has a large size and low electronegativity (2.96), it also has a low binding energy to carbon. Yet many researchers managed to grow it by different routes.<sup>[93,134]</sup> Recently Br-doped graphene with a doping level of 1.8 at% was reported by some authors of the present review article. In their direct one-step CVD procedure (Figure 7a,b), the configuration of the inner reactor tube played a significant role in the controlled growth. A single solid precursor (hexabromocyclododecane) was decomposed to simultaneously provide carbon and bromine. The temperature of the substrate sublimation was optimized to promote growth of continuous monolayer graphene with a large area and enhanced quality. Raman, SEM, and TEM studies evidenced single layer growth at the optimum precursor temperature of 200 °C (Figure 7c–f). The bromine was found to exist in both covalent and adsorbed forms.<sup>[46]</sup> In light of these observations, the parameters of precursor sublimation could be adjusted to efficiently prepare high-quality monolayer doped graphene. This work also highlights the importance of the vapor trapping CVD configuration.<sup>[135]</sup>

#### 4.8. N/O Codoped Graphene

As a single dopant, N binds strongly with graphene. It has also been used as a codopant with B, S, Al, etc.<sup>[136–138]</sup> On the other hand, the combination of nitrogen with oxygen species is less reported, especially its direct synthesis by CVD. An adapted

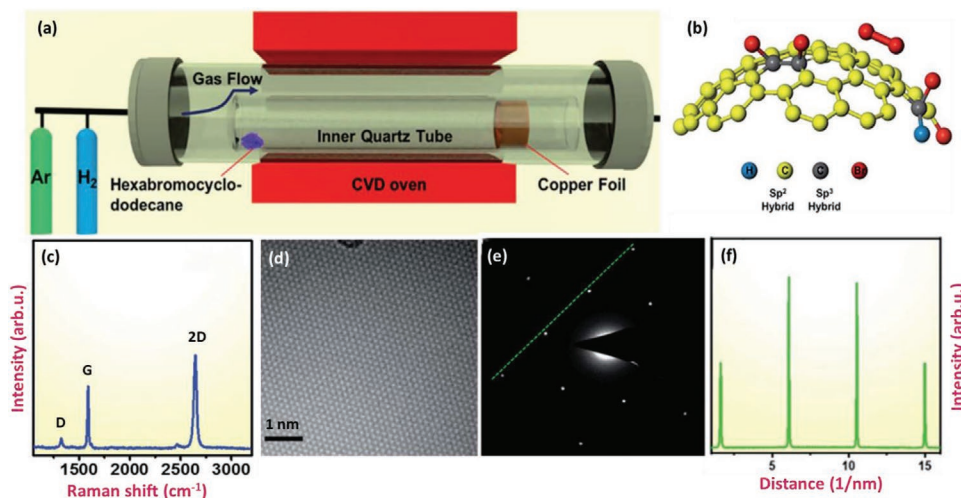


**Figure 7.** a) Schematic of CVD growth of Br-doped graphene. b) The corresponding stick-and-ball model of bromine-incorporated graphene. c–f) The respective Raman, HRTEM, SAED, and intensity profile of single-layer Br-doped graphene prepared at the optimal temperature (200 °C). Adapted with permission.<sup>[46]</sup> Copyright 2019, Royal Society of Chemistry.

vapor trapping CVD route (mentioned in Section 4.5 for bromine doping),<sup>[46]</sup> can also produce synthetic graphene that incorporates both nitrogen and O moieties. Here, three growth parameters were optimized to grow high-quality graphene at a precursor mass of 0.5 mg, a precursor sublimation temperature of 380 °C, and a growth duration of 3 min. In terms of the chemical state, graphitic, pyridinic, pyrrolic, pyridinic oxides, and oxygen species directly bound to carbon were all present. This CVD approach using an internal tube configuration may be developed into an established scalable synthetic technique.<sup>[77]</sup>

#### 4.9. Other Chemical Doping

In addition to the elemental doping of graphene reviewed above, there are many reports on modifying the properties of graphene by contacting it with chemically reactive agents. The graphene could be functionalized either covalently (e.g., hydroxyl group) or noncovalently (e.g., drugs). Noncovalent interactions is vital for the immobilization of DNA, proteins, and enzymes.<sup>[7,139–141]</sup> The interaction between the functional moieties and graphene tends to disrupt the regular electronic density of graphene, but the carbon in graphene is not expected to be substituted as generally observed in elemental doping. Shivananju et al. reported that biomolecules could be used similar to conventional functional molecules to chemically modify graphene.<sup>[142]</sup>

Furthermore, graphene-based composite/hybrid materials have attracted great attention due to the 2D structure of graphene.<sup>[143–145]</sup> Particularly, semiconductor nanocrystals or quantum dots with blended graphene or heterographene are extensively realized, such as silica nanocrystal/graphene composites.<sup>[146,147]</sup> Notably, although the carbon may not be replaced in these hybrid systems, disruption of the electron conjugation symmetry can lead to properties not observed in graphene itself, such as novel electromagnetic and photocatalytic characteristics.<sup>[148,149]</sup> In plenty of reports, these graphitic derivatives have presented remarkable applications ranging from energy generation to sensing and magnetic purposes.<sup>[150–154]</sup>

## 5. Recent Progresses in Applications of Doped Graphene

### 5.1. Energy-Related Applications

#### 5.1.1. Fuel Cells (ORR/Oxygen Evolution Reaction (OER)/Hydrogen Evolution Reaction (HER))

Economical, efficient, and durable metal-free catalysts are urgently needed in fuel cells to sustainably produce clean energy. A great amount of research (both experimentally<sup>[54]</sup> and theoretically<sup>[14,155,156]</sup>) has identified graphene, more precisely chemically doped graphene, as a candidate material for electrocatalysts. Doping breaks the inherently stable structure of pristine graphene to allow interaction with foreign species for catalysis. A high catalytic activity depends on the catalyst having a large accessible surface area, high electron mobility, suitable types of chemical dopants (mono- or codoping), doping level, chemical states, topological defects, and the creation of hybrid systems. Various strategies have been used to customize these features. For instance, a sulfur doping system demonstrated superior ORR efficiency,<sup>[65]</sup> with good durability and greater immunity against the methanol crossover effect and carbon monoxide (CO) poisoning as compared to Pt/C (Figure 8a–d). Previous studies suggested, that pyridinic N is more active in promoting ORR activity.<sup>[157]</sup> Miao and colleagues also found that pyridinic N substantially improves the stability of heteromaterials, which can lead to ORR catalysts with high durability.<sup>[110]</sup> Doped graphene (with metallic elements) heterosystems have also been exploited as ORR catalysts. Cr-doped graphene showed outstanding ORR activity and excellent stability.<sup>[52]</sup> Kumatani et al. took advantage of the combined effect of N/P dual doping and large numbers of edge sites. The edges had a high concentration of dopants, which greatly favored the catalytic reduction reaction. Rivera et al. experimentally tested N/S doping for ORR. The synergy between the two codopants led to better catalytic performance in alkaline than in acidic media. Also, the incorporation of N into the graphitic network

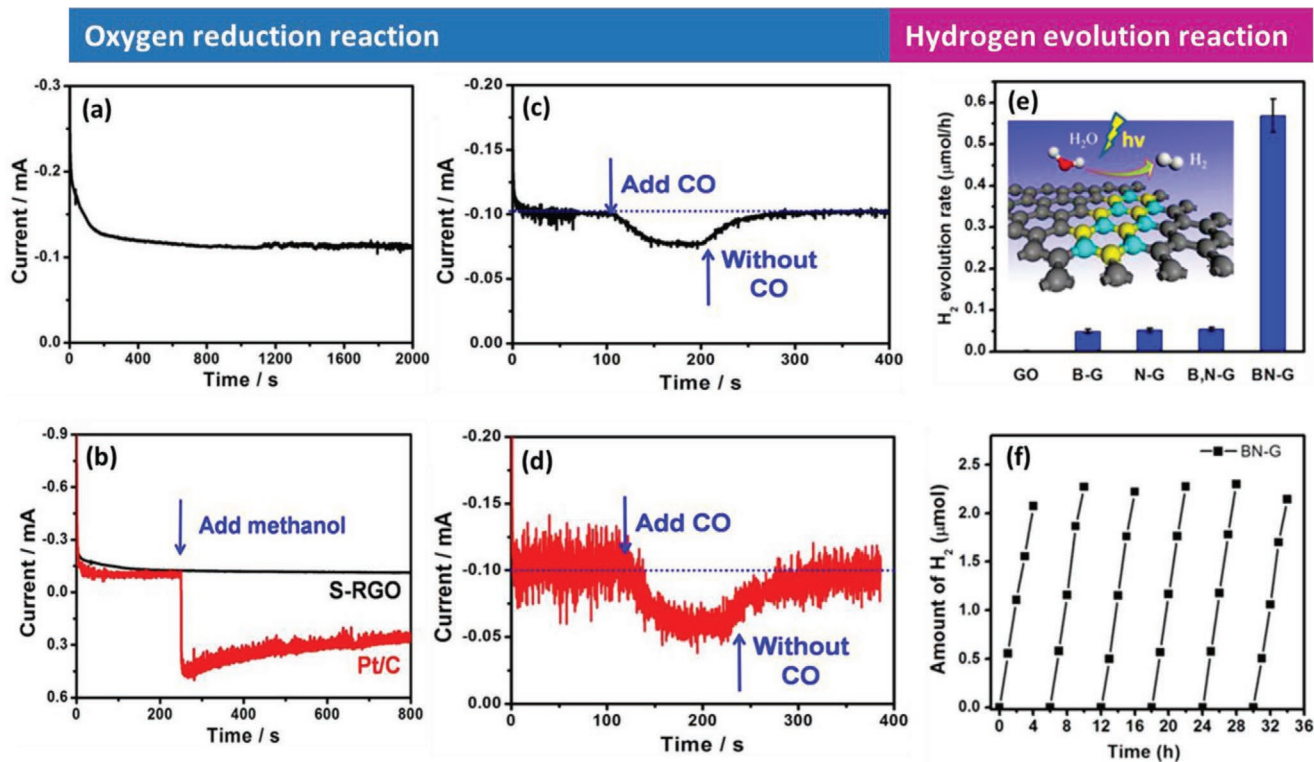


**Figure 8.** a) Steady-state chronoamperometric response of sulfur heterographene (S-rGO) as a catalyst at the polarizing potential of  $-0.3$  V in  $O_2$ -saturated electrolyte. b) Methanol crossover test of S-rGO and Pt/C catalysts, conducted by introducing 1.0 mL methanol into the electrolyte after 250 s of steady-state chronoamperometric response. Heterographene-based catalyst is clearly unaffected by methanol while Pt/C-based catalyst showed drastic decrease in current which demonstrate the stability of heterographene-based catalyst over metal-based. c,d) Carbon monoxide (CO) poisoning tests of rGO and Pt/C, conducted by introducing CO into the electrolyte. Again, sulfur-based graphene displayed greater immunity toward CO poisoning than Pt/C counterpart. a–d) Adapted with permission.<sup>[65]</sup> Copyright 2017, Elsevier. e) Hydrogen production activity over GO; B-G; N-G; B,N-G; and BN-G in photocatalytic hydrogen evolution. The inset is a schematic mechanism for hydrogen evolution from water on the surface of BN-G. f) Stability of BN-G during photocatalytic hydrogen evolution. Adapted with permission.<sup>[164]</sup> Copyright 2017, American Chemical Society.

facilitated the reaction by enhancing the adsorption and bond cleavage of  $O_2$ , favoring the direct four-electron pathway.<sup>[158]</sup> An Al/N dual doping system also demonstrated decent electrocatalytic activity for ORR, with not only higher electrocatalytic activity than commercial Pt/C but also adequate durability. Theoretical calculations showed that an inhomogeneous charge distribution and the interaction between Al and N are mainly responsible for the markedly enhanced ORR activity.<sup>[138]</sup> Some hybrid systems (composite materials) have offered greater ORR activities.<sup>[108]</sup> Zhang et al. demonstrated that  $Co_3O_4$  anchored N-doped rGO is a strong bifunctional catalyst for ORR and the OER due to the synergy between the inorganic component ( $Co_3O_4$ ) and the heterographitic N-rGO.<sup>[159]</sup> Because it is both cost-effective and efficient, this catalyst may replace the benchmark Pt/C catalyst in the near future.

On the other side, heterographene materials have also been considered as prospective OER catalysts from both theoretical and experimental perspectives.<sup>[160]</sup> Razmjooei and colleagues developed unique OER electrocatalysts by treating a range of heteroatom-doped graphene with iron (denoted as Fe-X-G; G = graphene, X = S, N, B, and P). The Fe-S-G system demonstrated the best activity among all the prepared catalysts. Fe serves two functions in this system, namely increasing the number of active sites and enhancing the conductivity, allowing

the Fe-S-G to catalyze OER with high efficiency. It is also worth mentioning that the OER activity of Fe-S-G is close to that of state-of-the-art  $IrO_2/C$  catalyst, along with pronounced long-term stability.<sup>[32]</sup> Many other chemically modified graphene derivatives with bifunctional catalytic abilities have been reported, some even exhibited multifunctional catalysis.<sup>[108,159]</sup> As an example, Cr-doped graphene is a very promising bifunctional catalyst, exhibiting outstanding OER and ORR activity and excellent stability.<sup>[52]</sup>

$H_2$  is a green energy source that can be produced by electrocatalytic water splitting. However, economical and efficient catalysts are still lacking for this reaction. Chemically doped graphene (singly doped, codoped, and even composite systems) have been researched using theoretical<sup>[161]</sup> and experimental means<sup>[117,162,163]</sup> to control their catalytic activities and comprehensively understand the catalytic mechanism. For instance, introducing chemical dopants and topological defects into the graphene framework is expected to synergistically promote the activity for HER over graphene. A highly active plasma-etched S-doped graphene (SG) catalyst was prepared through solvothermal synthesis followed by plasma-etching in an Ar atmosphere. The plasma etching could effectively introduce a high level of topological defects, while the doping creates a large number of active sites. Together, these steps significantly enhanced the HER activity of graphene.<sup>[26]</sup> In addition to single

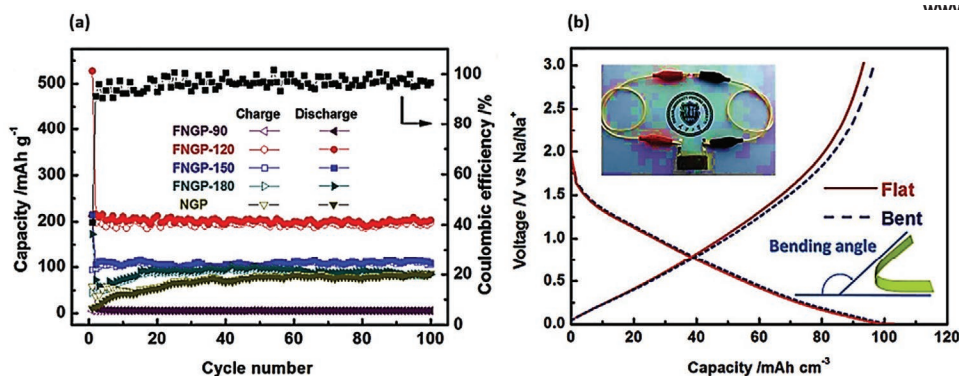


**Figure 9.** a) Cycling performance of fluorine-nitrogen co-doped graphene paper (FNGP) based electrode (FNGP-90, FNGP-120, FNGP-150 and FNGP-180, stands for FNGP treated at a range of solvothermal temperatures (90 °C, 120 °C, 150 °C and 180 °C respectively)) over a voltage range from 0.001 to 3.0 V at a current density of 50 mA g<sup>-1</sup>. FNGP-120 showed higher cycling performance or stability than its counterparts. b) Galvanostatic discharge/charge profiles in adaptable form (bend/flat conditions) of the pouch cell at a current density of 50 mA g<sup>-1</sup> (the inset is the photograph of the pouch cell). This feature demonstrate its superior mechanical strength and performance stability which is significant for wearable uses. Adapted with permission.<sup>[167]</sup> Copyright 2017, Elsevier.

doping and geometrical defects, some codoped systems also display a much enhanced catalytic performance. Li and co-workers developed N/B codoped graphene with h-BN patterns, and the H<sub>2</sub> evolution rate over this material was 10 times higher than that over the singly and codoped counterparts (Figure 7e). A photocatalyst based on h-BN displayed high stability in long-term H<sub>2</sub> production, as illustrated in Figure 7f.<sup>[164]</sup> Following the ideas of defect engineering and codoping, Kumatani et al. deployed SiO<sub>2</sub> nanoparticles (NPs) over the substrate to create holes when growing N/P dual-doped graphene. The purpose was to create more catalytic sites. As expected, the N/P codoped graphene had a large number of defects and also displayed remarkable HER activity.<sup>[157]</sup>

From these reports, it can be clearly seen that heteroatom doping and rational engineering of topological defects could produce graphene materials with superior catalytic performance in all three major energy-related reactions (ORR, OER, and HER). These materials may eventually replace commercial noble metal-based catalysts.

### 5.1.2. Batteries

Heterographitic materials are strong candidates in secondary batteries (e.g., lithium-ion (LiBs), sodium-ion (SiBs), and lithium-sulfur batteries (LiSs)) because of their large storage capacities, stability, light weight, and mechanical flexibility.<sup>[165]</sup> Chen et al. theoretically and experimentally examined the mechanism of lithiophilicity in various heterodoped graphene materials. They concluded, that the O-doped and O/B-doped systems exhibited the best lithiophilicity among single and codoping systems, respectively.<sup>[166]</sup> Moreover, metal-doped graphene has also shown advantages in LiBs by having topographical defects, increased wettability (electrodes based on doped graphene favorably interact with the electrolyte, which is critical for superior electrochemical energy conversion), and improved intersheet distances. In particular, Cr-doping in graphene allows rapid surface Li<sup>+</sup> adsorption as well as ultrafast Li<sup>+</sup> diffusion and electron transport, making the doped graphene superior to conventional bulk electrode materials that are based on Li intercalation and

conversion reactions.<sup>[52]</sup> Some hybrid systems were also successfully tested in LiBs resulting to excellent performances.<sup>[146]</sup> Xia and co-workers observed superior synergy in a composite of N-doped graphene and MoS<sub>2</sub> sheets, which displayed a large capacity for reversible lithium storage (1025 mAh g<sup>-1</sup> at a current density of 100 mA g<sup>-1</sup> for 100 cycles without any notable decrease). This good performance was ascribed to the strong interaction between the MoS<sub>2</sub> and the graphitic part (N heterographene).<sup>[109]</sup> Moreover, SiBs are a promising alternative to LiBs for large-scale energy storage due to their inherent safety and the low cost of sodium.<sup>[25,167]</sup> Singly or codoped graphene materials have shown excellent performance in SiBs.<sup>[67]</sup> On the other hand, Xiong et al. developed a hybrid system (Sb<sub>2</sub>S<sub>3</sub> on S-doped graphene) with a stable capacity retention of 83% for 900 cycles. Moreover, the Sb<sub>2</sub>S<sub>3</sub>/SG composite showed superior cycling performance in SiBs compared to other reported Sb-based materials. A computational study attributed the outstanding cycling stability to a robust composite architecture, pointing out a feasible and effective way to resolve the long-term cycling stability issue of SiBs.<sup>[168]</sup> Besides, F/N codoping of the graphene framework simultaneously increases the structural defects, provides active sites, and expands the graphene interlayer distance, all of which help improve the sodium ion storage capability. More importantly, the greater performance of this electrode in the bent state suggests potential applications in adaptable and wearable devices (see Figure 9a,b).<sup>[167]</sup> The LiS battery is another promising type of battery, due to its high energy density (2500 Wh kg<sup>-1</sup> or 2800 Wh L<sup>-1</sup>), high theoretical capacity (1675 mAh g<sup>-1</sup>), excellent cycling stability, low cost, environment friendliness, and natural abundance of sulfur sources. Heterographene is a top candidate electrode material for LiS batteries. According to Yuan et al., cathodes based on pyridinic N-doped carbon displayed higher capacity and better cycling stability as compared to the pyrrolic and graphitic nitrogen configurations.<sup>[67]</sup>

### 5.1.3. Supercapacitors

Several intrinsic features of heterographene (large surface area, conductivity, adaptability, light weight, single-atom thickness,

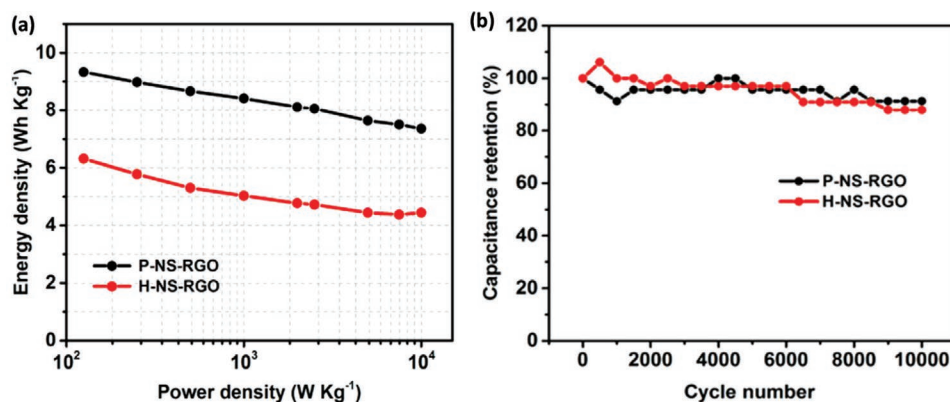


**Figure 10.** a) Ragone plot of plasma-treated and hydrothermally produced N/S codoped reduced graphene oxides (denoted by P-NS-RGO and H-NS-RGO, respectively). The former displayed a higher energy density. b) Cycling stability at the current density of 4 Ag<sup>-1</sup>. Adapted with permission.<sup>[31]</sup> Copyright 2019, American Chemical Society.

and especially the chemical doping) have inspired scientists to explore their potential in supercapacitors and ultracapacitors.<sup>[118]</sup> Graphene-based capacitors have exhibited high powder density, long durability, and flexibility. For instance, the boron monodoped system revealed a maximum specific capacitance retention of 93% through 10 000 cycles,<sup>[169]</sup> and the P/N codoped system demonstrated a capacity retention of 101% after 1000 cycles.<sup>[170]</sup> The single doping systems were further extended to include nitrogen and halogen heterodoping arrangements and even hybrid systems and in each system, the reported capacitive efficiency was higher. For instance, Cl-doped graphene (rGO) with high specific capacitance and good cycling stability is a promising electrode material for high-performance supercapacitors.<sup>[132]</sup> A hybrid system of N-doped graphene and the ionic liquid urea choline chloride is also considered promising electrode material for high-performance supercapacitors with good cycling stability and high specific capacitance.<sup>[171]</sup> In another case, the fluorine doping system was combined with amorphous carbon in a composite that showed better capacitance preservation (64%), and the capacitance was completely retained after 10 000 cycles in stability test. Such excellent supercapacitive performance suggests potentials use as electrode materials in energy storage devices.<sup>[172]</sup> Miao et al. employed the N/S codoping system as ultracapacitor electrode materials and demonstrated high performance. Those authors compared hydrothermally prepared and plasma-treated samples. As expected, the plasma-treated system showed better performance (Figure 10a,b).<sup>[31]</sup> In another study, the N/S codoped sample demonstrated excellent long-term cyclic stability (95% capacitive retention after 10 000 cycles) in capacitive performance. The excellent capacitive characteristics coupled with its simple and economic preparation technique imply great potential for N/S heterostructures in the field of energy storage.<sup>[173]</sup> Similarly, a B/N codoping system was reported to have excellent cyclic stability, retaining 94.8% of its initial capacitance after 10 000 cycles.<sup>[174]</sup>

## 5.2. Sensing of Gas and Dyes

Graphene is exceptionally inert and has only minimal interaction with other substances. However, chemical doping can

introduce active sensing sites into graphene. Many heterodoped graphene materials show great sensing capabilities. N-doped graphene has been employed to detecting dyes such as Rhodamine B (RhB), crystal violet (CRV), and methylene blue (MB). Upon interaction with dye molecules, the N-doped graphene displays an enhanced Raman scattering effect (SE), and distinctive peaks could be used for detecting each kind of molecule.<sup>[33]</sup> This unique property should be exploited for the identification of other molecules.<sup>[12]</sup> Ammonia (NH<sub>3</sub>), a chemical widely used in various industries, is toxic and can injure the skin, eyes, and the respiratory system when it is present in air in trace amounts (> 25 ppm). For highly sensitive sensors of ammonia, Srivastava et al. found that B-doped graphene exhibited speedy response (high sensitivity) to ammonia and immediate recovery.<sup>[39]</sup> The determination of hydrogen peroxide (H<sub>2</sub>O<sub>2</sub>) has significance in both the industry and biological reactions. Zhang et al. proposed a composite system (Co<sub>3</sub>O<sub>4</sub> decorated N-doped graphene) for fast, accurate, and reliable detection of H<sub>2</sub>O<sub>2</sub>.<sup>[159]</sup> Graphene has also been widely investigated for sensing nitrogen dioxide (NO<sub>2</sub>), which is a tremendously harmful gas that not only causes acid rain but also severely damages the human respiratory system, even at levels of 1 ppb in air. So, it is imperative to develop ultrasensitive sensors to detect NO<sub>2</sub> at the ppb level or lower. Previous graphene-based sensors showed poor selectivity, as they responded to several other gases including water vapor.<sup>[62]</sup> Guo et al. developed S-doped graphene (SG) as NO<sub>2</sub> sensor, which exhibited high sensitivity to NO<sub>2</sub> in a wide range from 500 ppt to 100 ppm at room temperature. Using the heater integrated system (micro-hot-platform), the signal from the SG sensors speedily recovered to the baseline within 5 min. Furthermore, the SG sensor exhibited excellent selectivity for NO<sub>2</sub> and minimal humidity effect, which is another requirement for practical applications (see Figure 11a–c).<sup>[86]</sup>

## 5.3. Optical and Optoelectronic Applications

Doped graphene tends to be sensitive to light in different ways, which enable their use in optoelectronic devices to generate, control, and detect lights.<sup>[175,176]</sup> Examples include light emitting diodes, laser diodes, photodiodes, and solar cells.<sup>[177,178]</sup>

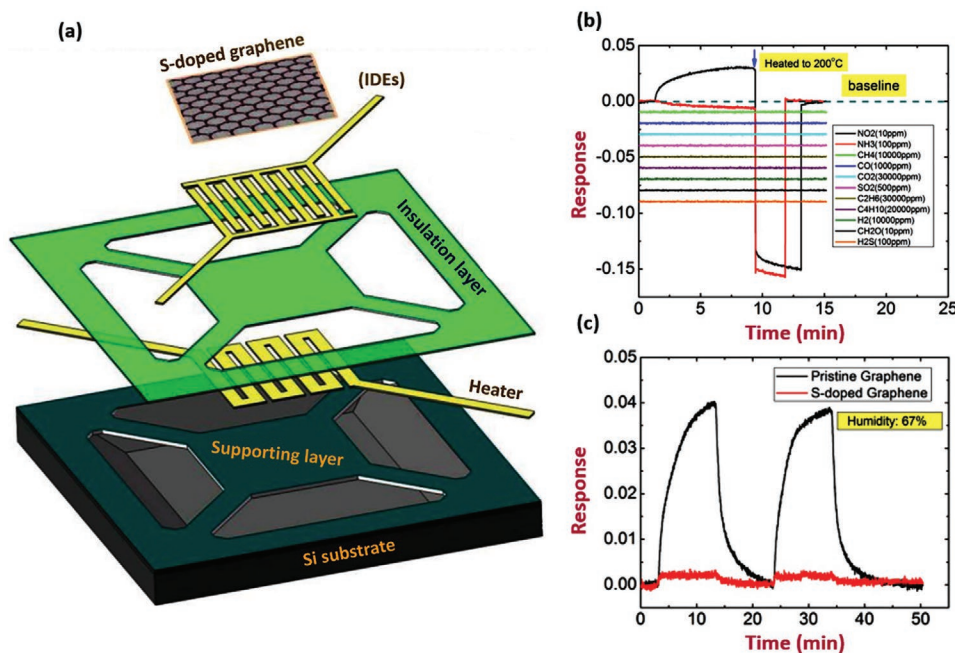


**Figure 11.** a) Expanded view of the micro-hotplatform (MHP) based sulfur doped graphene sensor displaying the parts. IDEs stands for interdigital electrodes. b) Response of Sulfur integrated graphene sensor to different gases. The sensor has good selectivity for  $\text{NO}_2$ . c) Repeated response of sulfur doped and pristine graphene based sensor to  $\text{H}_2\text{O}$  (humidity: 67% at 25 °C). Doped graphene is unaffected by humidity unlike the pristine graphene counterpart. Adapted with permission.<sup>[86]</sup> Copyright 2018, Elsevier.

The advantages offered by graphitic materials include improved photo-responses, as well as the fabrication of adaptable devices that are imperative for light-based and wearable technology. It has been predicted that singly doped heterographene (e.g., boron, nitrogen, silicon, aluminum, and phosphorous) and codoping systems (nitrogen-beryllium, N/Be) display useful light-matter interactions.<sup>[71,179–181]</sup> Interestingly, Wu et al. realized such photo-response in boron-doped graphene, exhibiting significant performance in organic light emitting diodes (OLEDs) with a record external quantum efficiency of 24.6% (Figure 12a–c). Thus, it may become an alternative material in adaptable OLEDs.<sup>[119]</sup> Correspondingly, Gan et al. employed a combined film of polymeric carbon nitride and N-doped graphene. The as-fabricated device with heterographitic active material showed fast and stable photo-responses.<sup>[182]</sup> These properties have been extended to additional graphitic derivatives, e.g. hybrid materials<sup>[183,184]</sup> and GQDs.<sup>[185,186]</sup>

#### 5.4. Bio-Related Applications

Recently, graphene with integrated heteroatoms has shown great promise in various bio-inspired applications. Single doped graphene (S-doping) was employed for detecting the biomarker 8-hydroxy-2-deoxyguanosine (8-OHdG), as illustrated in Figure 13a. The research-scale device with a doping level of 2.28 at% showed excellent sensitivity, high stability, and superior durability (Figure 13b,c). The thiophenic sulfur configuration was found to be the chemical state mainly responsible for 8-OHdG detection.<sup>[35]</sup> This approach strongly suggests that heterographene with bio-related potentials are economical,

efficient, and have commercial potential. Graphitic heteromaterials are efficient contenders for probing DNAs and their structural dynamics.<sup>[187,188]</sup> Recently, Shivananju and teammates used doped graphene to probe DNA molecules. Unlike the conventional probing techniques, the developed method was ultrafast, highly sensitive, cost-effective, and required minimal sample consumption for potential applications in treating DNA-related diseases such as cancer.<sup>[142]</sup>

The human body has to carefully control glucose levels, and so efficient systems for glucose detection are always in great demand. Recently, Singh et al. applied Br-doped graphene to detect glucose in human blood serum. The detection limit was determined to be  $28.41 \times 10^{-3} \text{ M}$  at a Br doping level of 3 at%. In the same work, Br-doped graphene was also found to recognize  $\text{H}_2\text{O}_2$ , which is both an important molecule in biology and an active pollutant in the environment.<sup>[134]</sup> Kotal et al. examined the synergistic effects in heterodoped systems such as S/N codoped graphene, and utilized it as artificial actuators (artificial muscles that generate movement). The obtained material was cost effective, pliable, and highly durable for commercial use in bio-related adaptable devices, wearable electronics, and other applications requiring elastic materials.<sup>[58]</sup> Dopamine (DA) and uric acid (UA) play significant roles in the central nervous and hormonal systems. Abnormal levels of DA can be an indicator of certain neurodegenerative diseases like Alzheimer's and Parkinson's, whereas an elevated level of UA in the body fluid might precede out attacks. Zhang et al. developed a composite of bimetallic NPs and double-doped graphene (such as AuPt NPs incorporated in N/S codoped graphene) for the recognition of DA and UA. Due to the synergetic effects between the codoped system and bimetallic NPs, the modified electrode exhibited excellent electrocatalytic

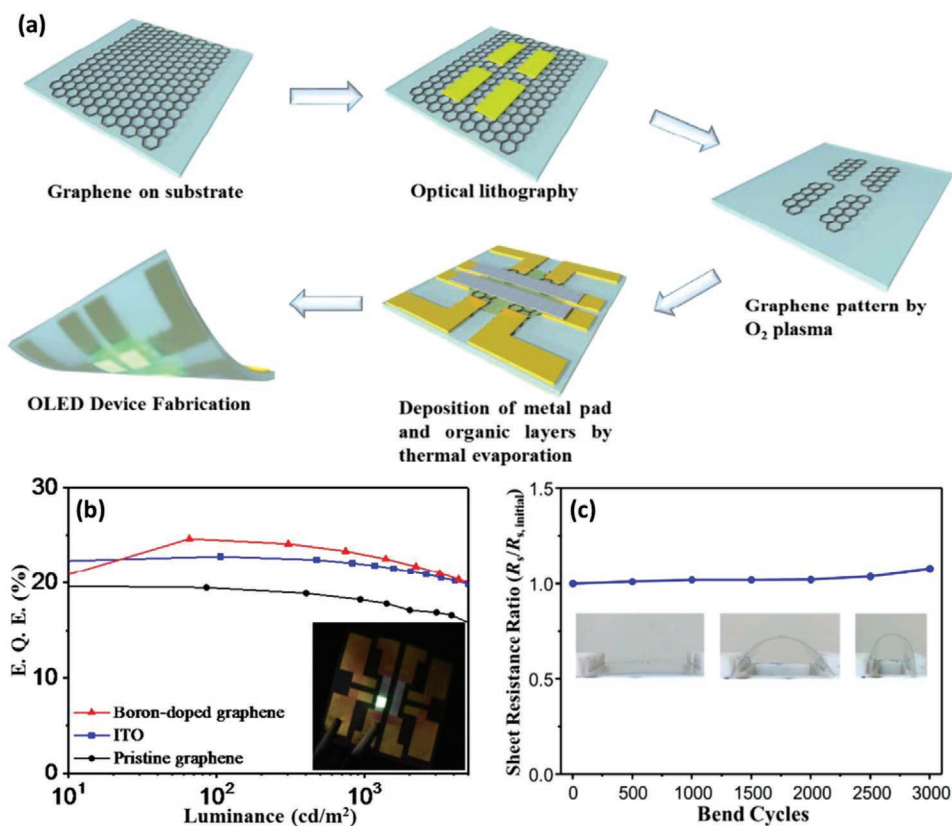


**Figure 12.** a) Schematic of OLED fabrication process. b) External quantum efficiency versus luminance for the boron-doped graphene OLED, ITO, and pristine graphene. Inset is the optical image of the OLED device. c) Sheet resistance ratio versus bending cycle of boron-doped graphene on PET. Inset: optical image of the test samples after different cycles of bending. Adapted with permission.<sup>[76]</sup> Copyright 2017, American Chemical Society.

properties toward the oxidation of DA and UA, and the respective detection limits were  $0.006$  and  $0.038 \times 10^{-6}$  M. With its excellent stability and reproducibility, this electrode could satisfactorily detect DA and UA in samples.<sup>[189]</sup>

### 5.5. Synthetic Uses

Chemical doping of carbon nanomaterials is a useful route to obtain reactive species that function as a secondary precursor for the post synthesis of useful grafted graphene derivatives. Halogenated graphene has attracted massive attention for this

reason. Covalently bound bromine, for instance, is an attractive synthetic handle and has been used to prepare PMMA grafted graphene. In addition, treatment with water and poly(ethylene glycol) methyl ether (mPEG) can functionalize bromine-doped graphene with hydroxyl (OH) and PEG groups (the as-grown materials are referred to as BrG-OH and BrG-PEG), respectively. This approach provides an easy way to access modified few layer graphene with improved and tunable dispersibility. Such modification is critical in bulk applications that require compatibility with common organic solvents, polymer matrices, and more importantly biocompatibility.<sup>[190]</sup> In addition, fluorine-incorporated graphene has shown comparable performance

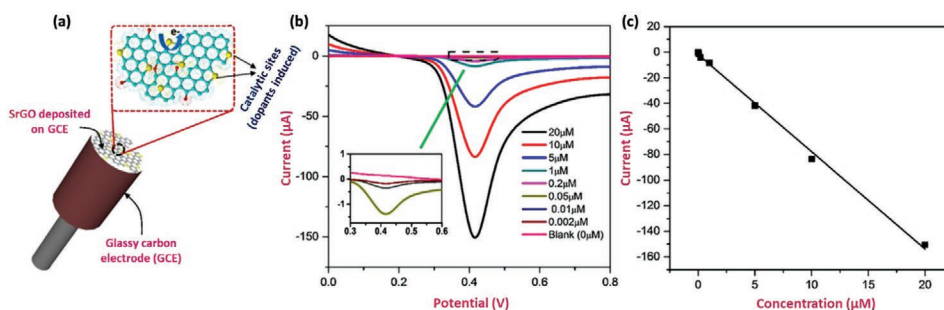


**Figure 13.** a) Schematic of sulfur-based sensor for 8-OHdG detection. b) Differential pulse voltammetry (DPV) responses of the sensor at different 8-OHdG concentrations. The inset is the expanded form of the square region in the DPV plot. c) Calibration curve for 8-OHdG concentrations between  $0.002$  and  $20 \times 10^{-6}$  M. Both plots indicate high sensitivity of the as-fabricated sensor. Adapted with permission.<sup>[35]</sup> Copyright 2016, Elsevier.

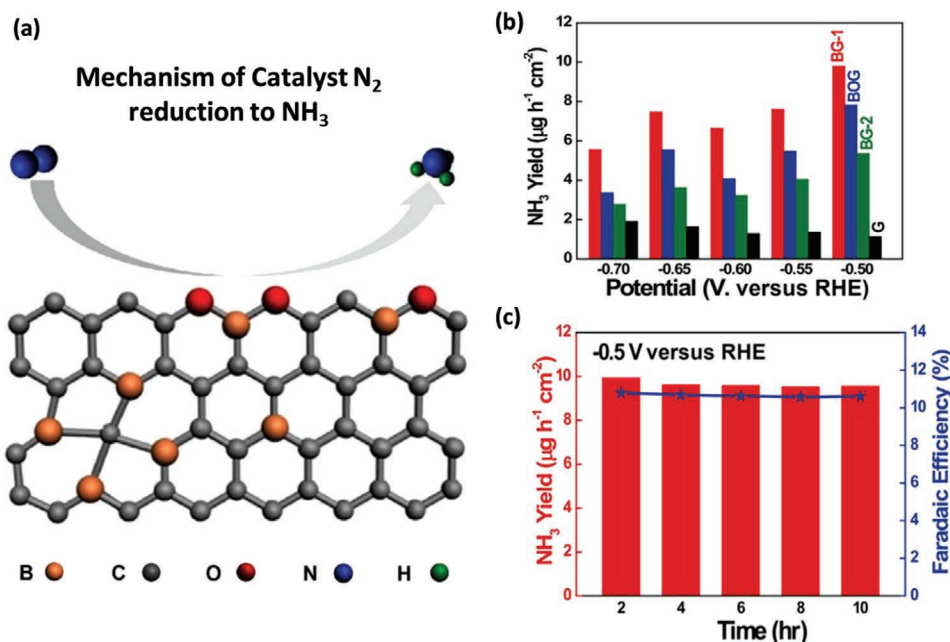


**Figure 14.** a) Schematic of the working mechanism for the electrocatalytic reduction of  $N_2$  to  $NH_3$ . b)  $NH_3$  production rates over BG-1, BOG, BG-2, and G at different potentials. c) Stability test of the optimal catalyst (BG-1) versus RHE. The boron-doped graphene was synthesized by mixing  $H_3BO_3$  and graphene oxides in different mass ratios (5:1, 1:10, and 0:1), and the respective samples were assigned as BG-1, BG-2, and G. Another BG catalyst grown under a high oxygen content is referred to as BOG. Adapted with permission.<sup>[94]</sup> Copyright 2018, Elsevier.

in the nucleophilic exchange of fluorine with aromatic thiol group. This approach could be used to modify the gapless electronic structure of graphene for electronic applications.<sup>[130]</sup> Ye et al. successfully modified fluorine-doped graphene (FG) by treatment with urea. The FG stayed on top of water when it is dispersed in accordance with its hydrophobic nature. On the other hand, the urea-functionalized FG became hydrophilic and could be properly dissolved in water. This suggests potential use in lubrication.<sup>[28]</sup> In light of this study, the authors concluded that heterodoped graphene (more precisely, halogenated graphene) materials are suitable secondary precursors for the synthesis of many useful graphene derivatives.

Ammonia, which is used in synthetic chemistry, agriculture, food industry, etc., is conventionally prepared using harsh conditions. To develop feasible, inexpensive, clean, and eco-friendly synthetic routes of ammonia, Yu et al. used graphene with covalently incorporated boron as electrocatalyst to promote the conversion of  $N_2$  to  $NH_3$ , as demonstrated in **Figure 14a**. The heterodoped graphene catalyst was highly efficient, with fivefold higher  $NH_3$  yield and superior stability compared to pure graphene (Figure 13b,c).<sup>[94]</sup> Heterodoped graphene composited with other materials has also presented tremendous potential as catalysts for producing useful chemicals. Cobalt-decorated N-doped graphene turned out to be unparalleled and robust for reducing quinoline compounds to the corresponding hydroquinoline derivatives, which are essential chemicals in agriculture and pharmaceuticals.<sup>[191]</sup>

## 5.6. Other Common Applications

Doped graphene has shown significant potential for many applications including in environmental, health, water, and

energy sectors. For example, due to its comparable size to carbon and reasonable electronegativity, boron has been used as a dopant in graphene for a wide range of applications. In particular, it was used for the photocatalytic degradation of organic pollutants such as methyl orange (MO) and methylene blue (MB). The heterosystem displayed the highest degradation potential, with complete degradation of MO and MB in 100 and 50 min, respectively. A theoretical study also emphasized the potential of boron-modified graphene as a catalyst in photodegradation, and this property can be exploited for other photocatalytic-based applications.<sup>[24]</sup> The applications of doped graphene continues to grow in number, attracting more and more attention from researchers. Recently, Arihanan et al. exploited the large surface area and storage capacity of nitrogen heterodoped graphene as a hydrogen ( $H_2$ ) storage material. At the N doping concentration of 75 at%, the  $H_2$  storage capacity at room temperature and 90 bar of pressure was 1.5 wt%.<sup>[192]</sup>

## 6. Future Outlook and Perspectives

Chemically doped heterographene has been studied in countless applications including electronics, catalysis, energy science, synthesis, sensing, and biorelated applications. Despite the significant advances, there remain questions in their synthesis and analysis. The conducting behavior and electronic characteristics also require further explanation (**Figure 15a–c**).

In terms of synthesis, a great deal of research effort was dedicated to growing continuous monolayer graphene with good quality and large area.<sup>[77]</sup> However, previous studies tend to be limited in scale and the results are often unsatisfactory.

Synthetic aspects; control over growth mechanism toward high-quality, large area and single layer doped graphene

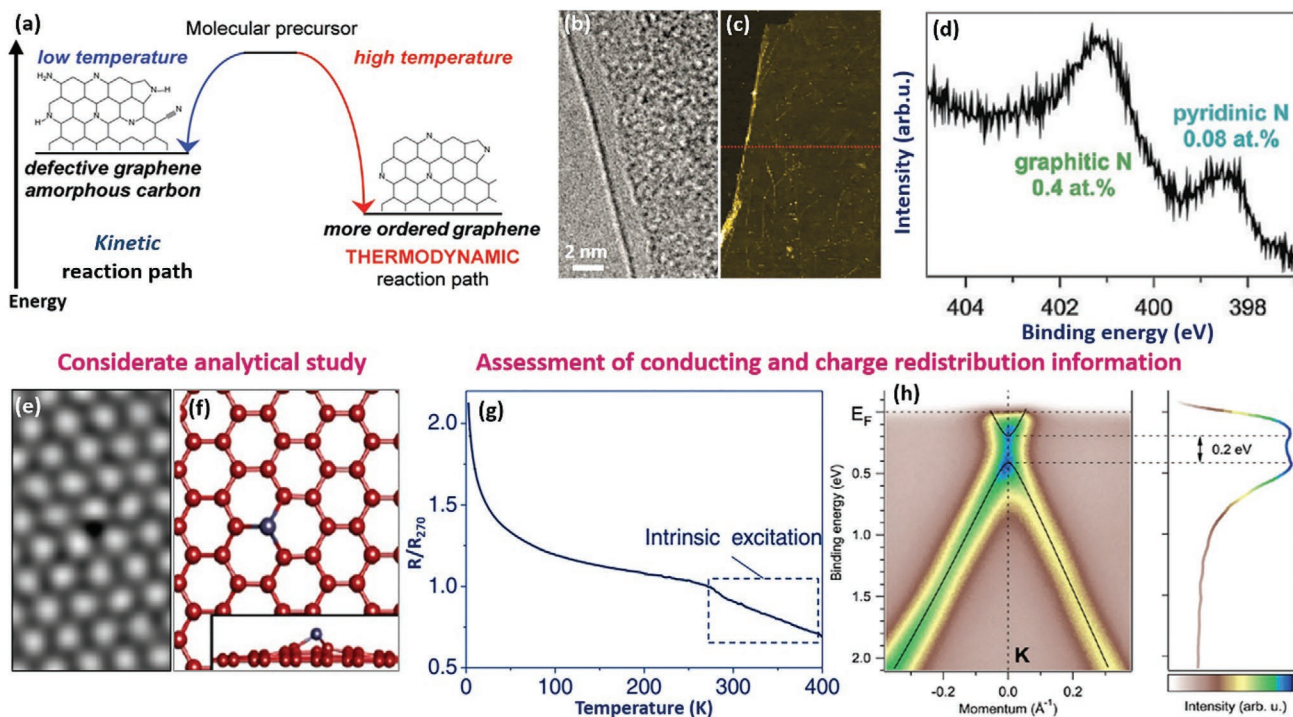


**Figure 15.** a–d) Further research question in synthesis: a) Growth pathway for nitrogen doped graphene at high and low temperatures in CVD mechanism. Adapted with permission.<sup>[200]</sup> Copyright 2014, American Chemical Society. b) HRTEM of single layer of nitrogen doped graphene. Adapted with permission.<sup>[201]</sup> Copyright 2015, American Chemical Society. c) AFM image of single layer nitrogen heterographene. Adapted with permission.<sup>[87]</sup> Copyright 2011, American Chemical Society. d) XPS spectrum of nitrogen incorporated graphene, showing the coexistence of graphitic and pyridinic N with the corresponding concentration. Control of the growth mechanism toward high-quality, large area, and single layer doped graphene with a particular doping configuration is critical for large-scale and reproducible applications, so, this area need the major focus from research communities. e, f) Further research question in analysis: e) Aberration-corrected TEM (AC-TEM) of iron doped graphene and, f) Corresponding DFT image. Adapted with permission.<sup>[127]</sup> Copyright 2013, American Chemical Society. Effective and more sensitive characterization methods up to the atomic scale (e.g., atomic resolution microscopy (STEM) and spectroscopy (EELS)) are extremely useful for obtaining accurate information about the structure, topographical features, and doping. g, h) Questions about conduction and charge redistribution: g) This plot highlight the change in resistance with respect to temperature of boron-based graphitic material. Adapted with permission.<sup>[195]</sup> Copyright 2012, Wiley-VCH. h) This figure indicates the band structure and corresponding bandgap ( $\approx 0.2$  eV) generated upon nitrogen integration to graphene. d, h) Adapted with permission.<sup>[59]</sup> Copyright 2011, American Chemical Society. These two properties significantly depend on the quality of graphene and the doping agent. Fundamental insight about them is necessary for developing the corresponding applications.

Specifically, no researcher has demonstrated the continuous growth of defectless monolayer graphene over a large area. The quality and thickness of graphene also strongly influence its conductivity, which in turn impacts the electrical and catalytic properties.<sup>[46,77]</sup> The ability to continuous grow graphene with a large area is helpful toward governing its conducting properties. In addition, the as-formed sample often contains a large amount of contamination and impurities from the growth and cleaning.<sup>[15,193]</sup> Therefore, it remains difficult to establish a reproducible synthetic route for a particular structure with a particular property.<sup>[41]</sup>

For instance, reports demonstrated that the catalytic functions can be promoted by chemical dopants, topographical defects, and/or other impurities, such as metal residues. Thus, a single characteristic is affected by several factors, and it is difficult to establish a one-to-one relationship between them.<sup>[40]</sup> Similarly, the introduction of doping agents causes inevitable defects that usually lower the conductivity and also destabilize the graphene. In other words, we need the ability to control a

target property in graphene by doping while preserving other intrinsic characteristics.

Other urgent issues in synthesis include controlling the doping mechanism and achieving a particular doping configuration, a degree of doping, and a tailored dopant distribution. To establish logical doping, various routes and the associated growth parameters have been optimized. However, many groups claimed controlled doping but none has been able to truly monitor these characteristics in the doped graphene. In the case of codoping, the scenario becomes even more complex due to the combined and synergistic/antagonistic effects from cobonding configurations.<sup>[18,57,160]</sup> There is great interest in developing viable and clean synthesis systems that are capable of such control and with high reproducibility.<sup>[41]</sup>

Many analytical techniques with high sensitivity are available to effectively evaluate the sample from various aspects. However, a thorough understanding of the structural information, specific doping features, and the corresponding properties remains elusive. In some cases, the instrument failed to detect

trace amounts of doped content, even though such a small amount would still affect the microelectronic properties.<sup>[59]</sup> Therefore, critical progresses are needed to enhance the sensitivity and precision of the analysis down to the atomic scale.

The third question regarding heterographene is understanding their conductive and electronic attributes in detail (Figure 15c). Despite extensive theoretical and experimental studies, the dependence of electron mobility and bandgap on the structural and doping attributes is still not fully known. In fact, multiple factors (such as the number of layers and the doping) jointly determine the conductivity,<sup>[194,195]</sup> whereas the electronic band structure is affected by the degree of doping and the different bonding configurations. Thus, the exact relationships are difficult to extract.<sup>[50]</sup> The rational design and reproducible production of given electronic structures should greatly facilitate the commercialization of heterographene materials.

We believe that the research of chemically doped graphene will continue to prosper, as a result of new opportunities presented by heteroatom doping. Besides the advancement of synthetic and analytical techniques, artificial intelligence (AI) can integrate self-rationality and automate graphene technology at the synthetic, characterization, and fabrication levels. Specifically, AI systems can automatically carry out/monitor heterographene growth and assess/correct the faults in order to produce high-quality graphene materials. While such incorporation of AI in graphene technology is still at its infancy, Leong et al. and Mendes et al. have suggested using AI in Raman and TEM studies, respectively.<sup>[91,196]</sup>

## 7. Conclusions

During chemical doping, noncarbon atoms are deliberately introduced into graphene. With their different electronegativity and size, the dopants cause rearrangement of the electronic band structure and activate the naturally inert graphene, resulting in the generation of a bandgap and a reactive structure that are key for the diverse applications of doped graphene. This article reviews various aspects of doped graphene, including the common analytical techniques and finally recent reported applications. Many doping agents could form multiple bonding configurations, each with unique properties. In terms of synthesis, the CVD method can produce continuous single layer doped graphene with excellent quality and large area, as well as exerting some control over the bonding configuration and rational design of the topographical defects. Similarly, ion implantation method could successfully introduce noncarbon atoms into the graphene lattice. For characterization purposes, atomic resolution microscopic (STEM) and spectroscopic studies (EELS) are favorable for assessment of graphene heterostructures by revealing information down to the atomic scale and even the electronic structure. Nevertheless, many questions about heterographene remain to be resolved, probably through the combination of theoretical, experimental, and analytical studies as well as artificial intelligence. The application prospects of heterographene will be greatly advanced if doped graphene with optimal structural and doping characteristics could be cheaply and reliably grown, and their structure–property relationships in the in situ state become firmly established.

## Acknowledgements

This work was financially supported by the National Science Foundation China (NSFC, Project No. 51672181) and the Czech Republic under the ERDF program “Institute of Environmental Technology—Excellent Research” (No. CZ.02.1.01/0.0/0.0/16\_019/0000853). M.H.R. and L.F. thank the Sino-German Research Institute for support (Project No. GZ 1400). M.H.R., J.C., and R.Y. are grateful for the funding provided by the Soochow Institute for Energy and Materials Innovations (SIEMIS) and the School of Energy, Suzhou University.

Open access funding enabled and organized by Projekt DEAL.

## Conflict of Interest

The authors declare no conflict of interest.

## Keywords

2D doped graphene, analytical approach, bonding configurations, properties, synthesis, various applications

Received: June 5, 2020

Revised: August 11, 2020

Published online: October 11, 2020

- [1] A. C. Ferrari, F. Bonaccorso, V. Fal'ko, K. S. Novoselov, S. Roche, P. Bøggild, S. Borini, F. H. Koppens, V. Palermo, N. Pugno, *Nanoscale* **2015**, *7*, 4598.
- [2] K. S. Novoselov, V. Fal, L. Colombo, P. Gellert, M. Schwab, K. Kim, *Nature* **2012**, *490*, 192.
- [3] W. Ren, H.-M. Cheng, *Nat. Nanotechnol.* **2014**, *9*, 726.
- [4] K. Chen, L. Shi, Y. Zhang, Z. Liu, *Chem. Soc. Rev.* **2018**, *47*, 3018.
- [5] M. H. Rummeli, E. Borowiak-Palen, T. Gemming, T. Pichler, M. Knupfer, M. Kalbác, L. Dunsch, O. Jost, S. R. P. Silva, W. Pompe, *Nano Lett.* **2005**, *5*, 1209.
- [6] M. H. Rummeli, A. Bachmatiuk, A. Scott, F. Borner, J. H. Warner, V. Hoffman, J.-H. Lin, G. Cuniberti, B. Buchner, *ACS Nano* **2010**, *4*, 4206.
- [7] G. Gao, D. Liu, S. Tang, C. Huang, M. He, Y. Guo, X. Sun, B. Gao, *Sci. Rep.* **2016**, *6*, 20034.
- [8] S. Kundu, V. K. Pillai, *Pillai, Phys. Sci. Rev.* **2019**, *5*.
- [9] I. V. Vlassiouk, Y. Stehle, P. R. Pudasaini, R. R. Unocic, P. D. Rack, A. P. Baddorf, I. N. Ivanov, N. V. Lavrik, F. List, N. Gupta, *Nat. Mater.* **2018**, *17*, 318.
- [10] A. J. Marsden, P. Brommer, J. J. Mudd, M. A. Dyson, R. Cook, M. Asensio, J. Avila, A. Levy, J. Sloan, D. Quigley, G. R. Bell, N. R. Wilson, *Nano Res.* **2015**, *8*, 2620.
- [11] S. Ullah, M. Hasan, H. Q. Ta, L. Zhao, Q. Shi, L. Fu, J. Choi, R. Yang, Z. Liu, M. H. Rummeli, *Adv. Funct. Mater.* **2019**, *29*, 1904457.
- [12] R. Lv, Q. Li, A. R. Botello-Méndez, T. Hayashi, B. Wang, A. Berkdemir, Q. Hao, A. L. Elías, R. Cruz-Silva, H. R. Gutiérrez, Y. A. Kim, H. Muramatsu, J. Zhu, M. Endo, H. Terrones, J.-C. Charlier, M. Pan, M. Terrones, *Sci. Rep.* **2012**, *2*, 586.
- [13] Y.-B. Tang, L.-C. Yin, Y. Yang, X.-H. Bo, Y.-L. Cao, H.-E. Wang, W.-J. Zhang, I. Bello, S.-T. Lee, H.-M. Cheng, C. S. Lee, *ACS Nano* **2012**, *6*, 1970.
- [14] F. Li, H. Shu, X. Liu, Z. Shi, P. Liang, X. Chen, *J. Phys. Chem. C* **2017**, *121*, 14434.
- [15] M. Tripathi, A. Markevich, R. Böttger, S. Facsko, E. Besley, J. Kotakoski, T. Susi, *ACS Nano* **2018**, *12*, 4641.
- [16] H. Wang, T. Maiyalagan, X. Wang, *ACS Catal.* **2012**, *2*, 781.

- [17] M. D. Esrafil, *Chem. Phys. Lett.* **2018**, *708*, 94.
- [18] A. Zitolo, V. Goellner, V. Armel, M.-T. Sougrati, T. Mineva, L. Stievano, E. Fonda, F. Jaouen, *Nat. Mater.* **2015**, *14*, 937.
- [19] M. Craciun, I. Khrapach, M. Barnes, S. Russo, *J. Phys. Condens. Matter* **2013**, *25*, 423201.
- [20] M. Del Cueto, P. Ocón, J. Poyato, *J. Phys. Chem. C* **2015**, *119*, 2004.
- [21] L. Qu, Y. Liu, J.-B. Baek, L. Dai, *ACS Nano* **2010**, *4*, 1321.
- [22] S. Agnoli, M. Favaro, *J. Mater. Chem. A* **2016**, *4*, 5002.
- [23] D. Y. Usachov, A. V. Fedorov, A. E. Petukhov, O. Y. Vilkov, A. G. Rybkin, M. M. Otrokov, A. Arnau, E. V. Chulkov, L. V. Yashina, M. Farjam, V. K. Adamchuk, B. V. Senkovskiy, C. Laubschat, D. V. Vyalikh, *ACS Nano* **2015**, *9*, 7314.
- [24] M. Singh, S. Kaushal, P. Singh, J. Sharma, *J. Photochem. Photobiol., A* **2018**, *364*, 130.
- [25] J. Yang, X. Zhou, D. Wu, X. Zhao, Z. Zhou, *Adv. Mater.* **2017**, *29*, 1604108.
- [26] Y. Tian, Z. Wei, X. Wang, S. Peng, X. Zhang, W.-m. Liu, *Int. J. Hydrogen Energy* **2017**, *42*, 4184.
- [27] Z. Bai, L. Zhang, L. Liu, *Nanoscale* **2016**, *8*, 8761.
- [28] X. Ye, L. Ma, Z. Yang, J. Wang, H. Wang, S. Yang, *ACS Appl. Mater. Interfaces* **2016**, *8*, 7483.
- [29] X. Mu, B. Yuan, X. Feng, S. Qiu, L. Song, Y. Hu, *RCS Adv.* **2016**, *6*, 105021.
- [30] J. Xi, Q. Wang, J. Liu, L. Huan, Z. He, Y. Qiu, J. Zhang, C. Tang, J. Xiao, S. Wang, *J. Catal.* **2018**, *359*, 233.
- [31] Y. Miao, Y. Ma, Q. Wang, *ACS Sustainable Chem. Eng.* **2019**, *7*, 7597.
- [32] F. Razmjooei, K. P. Singh, D.-S. Yang, W. Cui, Y. H. Jang, J.-S. Yu, *ACS Catal.* **2017**, *7*, 2381.
- [33] S. Feng, M. C. dos Santos, B. R. Carvalho, R. Lv, Q. Li, K. Fujisawa, A. L. Elias, Y. Lei, N. Perea-López, M. Endo, *Sci. Adv.* **2016**, *2*, e1600322.
- [34] M. Legesse, S. N. Rashkeev, F. Al-Dirini, F. H. Alharbi, *Appl. Surf. Sci.* **2020**, *509*, 144893.
- [35] F. Shahzad, S. A. Zaidi, C. M. Koo, *Sens. Actuators, B* **2017**, *241*, 716.
- [36] H. Gursu, M. Gencten, Y. Sahin, *Int. J. Electrochem. Sci.* **2018**, *13*, 875.
- [37] M. H. Rummeli, A. Bachmatiuk, A. Scott, F. Bornert, J. H. Warner, V. Hoffman, J.-H. Lin, G. Cuniberti, B. Buchner, *ACS Nano* **2010**, *4*, 4206.
- [38] J. Zhang, C. Zhao, N. Liu, H. Zhang, J. Liu, Y. Q. Fu, B. Guo, Z. Wang, S. Lei, P. A. Hu, *Sci. Rep.* **2016**, *6*, 28330.
- [39] S. Srivastava, S. K. Jain, G. Gupta, T. Senguttuvan, B. K. Gupta, *RSC Adv.* **2020**, *10*, 1007.
- [40] J. Duan, S. Chen, M. Jaroniec, S. Z. Qiao, *ACS Catal.* **2015**, *5*, 5207.
- [41] X. Wang, G. Sun, P. Routh, D.-H. Kim, W. Huang, P. Chen, *Chem. Soc. Rev.* **2014**, *43*, 7067.
- [42] C. Maddi, F. Bourquard, V. Barnier, J. Avila, M.-C. Asensio, T. Tite, C. Donnet, F. Garrelie, *Sci. Rep.* **2018**, *8*, 3247.
- [43] K. C. Wasalathilake, G. A. Ayoko, C. Yan, *Carbon* **2018**, *140*, 276.
- [44] Q. M. Ramasse, C. R. Seabourne, D.-M. Kepaptsoglou, R. Zan, U. Bangert, A. J. Scott, *Nano Lett.* **2013**, *13*, 4989.
- [45] M. Yang, L. Zhou, J. Wang, Z. Liu, Z. Liu, *J. Phys. Chem. C* **2012**, *116*, 844.
- [46] M. Hasan, W. Meiou, L. Yulian, S. Ullah, H. Q. Ta, L. Zhao, R. G. Mendes, Z. P. Malik, N. M. Ahmad, Z. Liu, *RSC Adv.* **2019**, *9*, 13527.
- [47] M. Park, I.-Y. Jeon, J. Ryu, H. Jang, J.-B. Back, J. Cho, *Nano Energy* **2016**, *26*, 233.
- [48] J. Zheng, H.-T. Liu, B. Wu, C.-A. Di, Y.-L. Guo, T. Wu, G. Yu, Y.-Q. Liu, D.-B. Zhu, *Sci. Rep.* **2012**, *2*, 662.
- [49] F. S. Karlický, K. Kumara Ramanatha Datta, M. Otyepka, R. Zboril, *ACS Nano* **2013**, *7*, 6434.
- [50] J. Mach, P. Procházka, M. Bartošík, D. Nezval, J. Piastek, J. Hulva, V. Švarc, M. Konečný, L. Kormoš, T. Šíkola, *Nanotechnology* **2017**, *28*, 415203.
- [51] S. S. Varghese, S. Swaminathan, K. K. Singh, V. Mittal, *Comput. Condens. Matter* **2016**, *9*, 40.
- [52] Z. Kou, T. Meng, B. Guo, I. S. Amiinu, W. Li, J. Zhang, S. Mu, *Adv. Funct. Mater.* **2017**, *27*, 1604904.
- [53] Z. He, K. He, A. W. Robertson, A. I. Kirkland, D. Kim, J. Ihm, E. Yoon, G.-D. Lee, J. H. Warner, *Nano Lett.* **2014**, *14*, 3766.
- [54] A. Arunchander, S. G. Peera, S. K. Panda, S. Chellammal, A. Sahu, *Carbon* **2017**, *118*, 531.
- [55] H. Yuan, H. Chen, D. Li, L. Deng, J. Chen, Y. Fan, M. He, F. Sun, *Electrochem. Commun.* **2019**, *100*, 52.
- [56] G. Bepete, D. Voiry, M. Chhowalla, Z. Chiguvare, N. Coville, *Nanoscale* **2013**, *5*, 6552.
- [57] L. Ci, L. Song, C. Jin, D. Jariwala, D. Wu, Y. Li, A. Srivastava, Z. Wang, K. Storr, L. Balicas, *Nat. Mater.* **2010**, *9*, 430.
- [58] M. Kotal, J. Kim, K. J. Kim, I. K. Oh, *Adv. Mater.* **2016**, *28*, 1610.
- [59] D. Usachov, O. Vilkov, A. Gruneis, D. Haberer, A. Fedorov, V. Adamchuk, A. Preobrajenski, P. Dudin, A. Barinov, M. Oehzelt, *Nano Lett.* **2011**, *11*, 5401.
- [60] D. Wei, Y. Liu, Y. Wang, H. Zhang, L. Huang, G. Yu, *Nano Lett.* **2009**, *9*, 1752.
- [61] M. Ovezmyradov, I. V. Magedov, L. V. Frolova, G. Chandler, J. Garcia, D. Bethke, E. A. Shaner, N. G. Kalugin, *J. Nanosci. Nanotechnol.* **2015**, *15*, 4883.
- [62] R. Lv, G. Chen, Q. Li, A. McCreary, A. Botello-Méndez, S. Morozov, L. Liang, X. Declerck, N. Perea-López, D. A. Cullen, *Proc. Natl. Acad. Sci. USA* **2015**, *112*, 14527.
- [63] J. Zhang, C. Zhao, N. Liu, H. Zhang, J. Liu, Y. Q. Fu, B. Guo, Z. Wang, S. Lei, P. Hu, *Sci. Rep.* **2016**, *6*, 28330.
- [64] M. Scardamaglia, C. Struzzi, S. Osella, N. Reckinger, J.-F. Colomer, L. Petaccia, R. Snyders, D. Beljonne, C. Bittencourt, *2D Mater.* **2016**, *3*, 011001.
- [65] C. Zhai, M. Sun, M. Zhu, S. Song, S. Jiang, *Appl. Surf. Sci.* **2017**, *407*, 503.
- [66] H. Q. Ta, L. Zhao, W. Yin, D. Pohl, B. Rellinghaus, T. Gemming, B. Trzebiecka, J. Palisaitis, G. Jing, P. O. Persson, Z. Liu, A. Bachmatiuk, M. H. Rummeli, *Nano Res.* **2018**, *11*, 2405.
- [67] H. Yuan, W. Zhang, J.-G. Wang, G. Zhou, Z. Zhuang, J. Luo, H. Huang, Y. Gan, C. Liang, Y. Xia, *Energy Storage Mater.* **2018**, *10*, 1.
- [68] R. Zbořil, F. Karlický, A. B. Bourlinos, T. A. Steriotis, A. K. Stubos, V. Georgakilas, K. Šafářová, D. Jančík, C. Trapalis, M. Otyepka, *Small* **2010**, *6*, 2885.
- [69] H. L. Poh, M. Pumera, *ChemElectroChem* **2015**, *2*, 190.
- [70] Y. Qin, H.-H. Wu, L. A. Zhang, X. Zhou, Y. Bu, W. Zhang, F. Chu, Y. Li, Y. Kong, Q. Zhang, *ACS Catal.* **2019**, *9*, 610.
- [71] O. Olaniyan, R. Maphasha, M. Madito, A. Khaleed, E. Igumbor, N. Manyala, *Carbon* **2018**, *129*, 207.
- [72] O. Olaniyan, R. E. Mapasha, D. Y. Momodu, M. Madito, A. Kahleed, F. Ugbo, A. Bello, F. Barzegar, K. Oyedotun, N. Manyala, *RSC Adv.* **2016**, *6*, 88392.
- [73] P. A. Denis, *Comput. Theor. Chem.* **2016**, *1097*, 40.
- [74] R. Ma, Y. Ma, Y. Dong, J.-M. Lee, *Nano Adv.* **2016**, *1*, 50.
- [75] H. Zhou, W. J. Yu, L. Liu, R. Cheng, Y. Chen, X. Huang, Y. Liu, Y. Wang, Y. Huang, X. Duan, *Nat. Commun.* **2013**, *4*, 2096.
- [76] T.-L. Wu, C.-H. Yeh, W.-T. Hsiao, P.-Y. Huang, M.-J. Huang, Y.-H. Chiang, C.-H. Cheng, R.-S. Liu, P.-W. Chiu, *ACS Appl. Mater. Interfaces* **2017**, *9*, 14998.
- [77] M. Hasan, W. Meiou, L. Yulian, H. Q. Ta, L. Zhao, R. G. Mendes, S. Oswald, Z. Akhter, Z. P. Malik, N. M. Ahmad, *Mater. Res. Express* **2019**, *6*, 055604.
- [78] K. N. Kim, V. P. Pham, G. Y. Yeom, *ECS J. Solid State Sci. Technol.* **2015**, *4*, N5095.
- [79] Z. Sun, Z. Yan, J. Yao, E. Beitler, Y. Zhu, J. M. Tour, *Nature* **2010**, *468*, 549.
- [80] Y. Xue, B. Wu, L. Jiang, Y. Guo, L. Huang, J. Chen, J. Tan, D. Geng, B. Luo, W. Hu, *J. Am. Chem. Soc.* **2012**, *134*, 11060.

- [81] K. Kanahashi, N. Tanaka, Y. Shoji, M. Maruyama, I. Jeon, K. Kawahara, M. Ishihara, M. Hasegawa, H. Ohta, H. Ago, Y. Matsuo, S. Okada, T. Fukushima, T. Takenobu, *npj 2D Mater. Appl.* **2019**, *3*, 1.
- [82] W. Cai, C. Wang, X. Fang, L. Yang, X. Chen, *Appl. Phys. Lett.* **2015**, *106*, 253105.
- [83] A. W. Robertson, J. H. Warner, *Nano Lett.* **2011**, *11*, 1182.
- [84] S. M. Shinde, E. Kano, G. Kalita, M. Takeguchi, A. Hashimoto, M. Tanemura, *Carbon* **2016**, *96*, 448.
- [85] J. H. Warner, E. R. Margine, M. Mukai, A. W. Robertson, F. Giustino, A. I. Kirkland, *Science* **2012**, *337*, 209.
- [86] L. Guo, T. Li, *Sens. Actuators, B* **2018**, *255*, 2258.
- [87] Z. Jin, J. Yao, C. Kittrell, J. M. Tour, *ACS Nano* **2011**, *5*, 4112.
- [88] H. Wang, Y. Zhou, D. Wu, L. Liao, S. Zhao, H. Peng, Z. Liu, *Small* **2013**, *9*, 1316.
- [89] X. Chen, R. Xiang, P. Zhao, H. An, T. Inoue, S. Chiashi, S. Maruyama, *Carbon* **2016**, *107*, 852.
- [90] F. Hofer, F.-P. Schmidt, W. Grogger, G. Kothleitner, *IOP Conf. Ser.: Mater. Sci. Eng.* **2016**, *109*, 1.
- [91] R. G. Mendes, J. Pang, A. Bachmatiuk, H. Q. Ta, L. Zhao, T. Gemming, L. Fu, Z. Liu, M. H. Rummeli, *ACS Nano* **2019**, *13*, 978.
- [92] I.-Y. Jeon, H.-J. Choi, M. Choi, J.-M. Seo, S.-M. Jung, M.-J. Kim, S. Zhang, L. Zhang, Z. Xia, L. Dai, N. Park, J. B. Baek, *Sci. Rep.* **2013**, *3*, 1810.
- [93] S. Lai, Y. Jin, X. Sun, J. Pan, W. Du, L. Shi, *Res. Chem. Intermed.* **2018**, *44*, 3523.
- [94] X. Yu, P. Han, Z. Wei, L. Huang, Z. Gu, S. Peng, J. Ma, G. Zheng, *Joule* **2018**, *2*, 1610.
- [95] C. Zhang, D. M. Dabbs, L.-M. Liu, I. A. Aksay, R. Car, A. Selloni, *J. Phys. Chem. C* **2015**, *119*, 18167.
- [96] T. Susi, T. P. Hardcastle, H. Hofsäss, A. Mittelberger, T. J. Pennycook, C. Mangler, R. Drummond-Brydson, A. J. Scott, J. C. Meyer, J. Kotakoski, *2D Mater.* **2017**, *4*, 021013.
- [97] W. Zhou, M. D. Kapetanakis, M. P. Prange, S. T. Pantelides, S. J. Pennycook, J.-C. Idrobo, *Phys. Rev. Lett.* **2012**, *109*, 206803.
- [98] A. W. Robertson, C. S. Allen, Y. A. Wu, K. He, J. Olivier, J. Neethling, A. I. Kirkland, J. H. Warner, *Nat. Commun.* **2012**, *3*, 1.
- [99] C. Hofer, V. Skákalová, T. Görlich, M. Tripathi, A. Mittelberger, C. Mangler, M. R. A. Monazam, T. Susi, J. Kotakoski, J. C. Meyer, *Nat. Commun.* **2019**, *10*, 4570.
- [100] D. Kepaptsoglou, T. P. Hardcastle, C. R. Seabourne, U. Bangert, R. Zan, J. A. Amani, H. Hofsäss, R. J. Nicholls, R. M. Brydson, A. J. Scott, *ACS Nano* **2015**, *9*, 11398.
- [101] A. W. Robertson, B. Montanari, K. He, C. S. Allen, Y. A. Wu, N. M. Harrison, A. I. Kirkland, J. H. Warner, *ACS Nano* **2013**, *7*, 4495.
- [102] O. Dyck, S. Kim, S. V. Kalinin, S. Jesse, *Appl. Phys. Lett.* **2017**, *111*, 113104.
- [103] M. Tripathi, A. Mittelberger, N. A. Pike, C. Mangler, J. C. Meyer, M. J. Verstraete, J. Kotakoski, T. Susi, *Nano Lett.* **2018**, *18*, 5319.
- [104] J. H. Warner, Y.-C. Lin, K. He, M. Koshino, K. Suenaga, *ACS Nano* **2014**, *8*, 11806.
- [105] L. Zhao, H. Q. Ta, R. G. Mendes, A. Bachmatiuk, M. H. Rummeli, *Adv. Mater. Interfaces* **2020**, *7*, 2000436.
- [106] S. Zhou, N. Liu, Z. Wang, J. Zhao, *ACS Appl. Mater. Interfaces* **2017**, *9*, 22578.
- [107] G. Sarau, M. Heilmann, M. Bashouti, M. Latzel, C. Tessarek, S. Christiansen, *ACS Appl. Mater. Interfaces* **2017**, *9*, 10003.
- [108] A. Pendashteh, J. Palma, M. Anderson, R. Marcilla, *Appl. Catal., B* **2017**, *201*, 241.
- [109] S. Xia, Y. Wang, Y. Liu, C. Wu, M. Wu, H. Zhang, *Chem. Eng. J.* **2018**, *332*, 431.
- [110] H. Miao, S. Li, Z. Wang, S. Sun, M. Kuang, Z. Liu, J. Yuan, *Int. J. Hydrog. Energy* **2017**, *42*, 28298.
- [111] Y. Xu, Y. Mo, J. Tian, P. Wang, H. Yu, J. Yu, *Appl. Catal., B* **2016**, *181*, 810.
- [112] C. D. Cress, S. W. Schmucker, A. L. Friedman, P. Dev, J. C. Culbertson, J. W. Lyding, J. Robinson, *ACS Nano* **2016**, *10*, 3714.
- [113] P. D. Kaushik, M. Rodner, G. Lakshmi, I. G. Ivanov, G. Greczynski, J. Palisaitis, J. Eriksson, P. Solanki, A. Aziz, A. M. Siddiqui, *Carbon* **2020**, *157*, 169.
- [114] T. Granzier-Nakajima, K. Fujisawa, V. Anil, M. Terrones, Y.-T. Yeh, *Nanomaterials* **2019**, *9*, 425.
- [115] Y. Zhao, X. Wang, E. Fu, D. Han, P. Wang, Z. Wu, Y. Chen, Y. Chen, Z. Zhao, *Carbon* **2018**, *139*, 732.
- [116] U. Bangert, W. Pierce, D. Kepaptsoglou, Q. Ramasse, R. Zan, M. Gass, J. Van den Berg, C. Boothroyd, J. Amani, H. Hofsäss, *Nano Lett.* **2013**, *13*, 4902.
- [117] L. K. Putri, B.-J. Ng, W.-J. Ong, H. W. Lee, W. S. Chang, S.-P. Chai, *ACS Appl. Mater. Interfaces* **2017**, *9*, 4558.
- [118] V. Thirumal, A. Pandurangan, R. Jayavel, R. Ilangovan, *Synth. Met.* **2016**, *220*, 524.
- [119] T.-L. Wu, C.-H. Yeh, W.-T. Hsiao, P.-Y. Huang, M.-J. Huang, Y.-H. Chiang, C.-H. Cheng, R.-S. Liu, P.-W. Chiu, *ACS Appl. Mater. Interfaces* **2017**, *9*, 14998.
- [120] T. Liang, Y. Kong, H. Chen, M. Xu, *Chin. J. Chem.* **2016**, *34*, 32.
- [121] Y. Bleu, F. Bourquard, V. Barnier, Y. Lefkir, S. Reynaud, A.-S. Loir, F. Garrelie, C. Donnet, *Appl. Surf. Sci.* **2020**, *513*, 145843.
- [122] A. Dianat, Z. Liao, M. Gall, T. Zhang, R. Gutierrez, E. Zschech, G. Cuniberti, *Nanotechnology* **2017**, *28*, 215701.
- [123] D. Boukhvalov, I. Zhidkov, A. Kukhareenko, A. Slesarev, A. Zatsepina, S. Cholakh, E. Kurmaev, *Appl. Surf. Sci.* **2018**, *441*, 978.
- [124] E. Romani, D. Larrude, M. da Costa, G. Mariotto, F. Freire, *J. Nanomater.* **2017**, *2017*, 9298637.
- [125] H. L. Poh, M. Pumera, *ChemElectroChem* **2015**, *2*, 190.
- [126] S.-M. He, C.-C. Huang, J.-W. Liou, W.-Y. Woon, C.-Y. Su, *ACS Appl. Mater. Interfaces* **2019**, *11*, 47289.
- [127] A. W. Robertson, B. Montanari, K. He, J. Kim, C. S. Allen, Y. A. Wu, J. Olivier, J. Neethling, N. Harrison, A. I. Kirkland, *Nano Lett.* **2013**, *13*, 1468.
- [128] G. Kalita, K. Wakita, M. Takahashi, M. Umeno, *J. Mater. Chem.* **2011**, *21*, 15209.
- [129] J. T. Robinson, J. S. Burgess, C. E. Junkermeier, S. C. Badescu, T. L. Reinecke, F. K. Perkins, M. K. Zalalutdniov, J. W. Baldwin, J. C. Culbertson, P. E. Sheehan, *Nano Lett.* **2010**, *10*, 3001.
- [130] P. Kovářiček, Z. Bastl, V. Valeš, M. Kalbac, *Chem. Eur. J.* **2016**, *22*, 5404.
- [131] L. Cheng, S. Jandhyala, G. Mordi, A. T. Lucero, J. Huang, A. Azcatl, R. Addou, R. M. Wallace, L. Colombo, J. Kim, *ACS Appl. Mater. Interfaces* **2016**, *8*, 5002.
- [132] K. Kakaei, M. Hamidi, S. Husseindoost, *J. Colloid Interface Sci.* **2016**, *479*, 121.
- [133] G. Copetti, E. H. Nunes, G. K. Rolim, G. V. Soares, S. A. Correa, D. E. Weibel, C. Radtke, *J. Phys. Chem. C* **2018**, *122*, 16333.
- [134] S. Singh, K. Mitra, R. Singh, A. Kumari, S. K. S. Gupta, N. Misra, P. Maiti, B. Ray, *Anal. Methods* **2017**, *9*, 6675.
- [135] M. H. Rummeli, S. Gorantla, A. Bachmatiuk, J. Pihler, N. Geissler, I. Ibrahim, J. Pang, J. Eckert, *Chem. Mater.* **2013**, *25*, 4861.
- [136] S. Elumalai, C. Y. Su, M. Yoshimura, *Front. Mater.* **2019**, *6*, 216.
- [137] L. Cheng, Y. Hu, D. Qiao, Y. Zhu, H. Wang, Z. Jiao, *Electrochim. Acta* **2018**, *259*, 587.
- [138] Y. Qin, H.-H. Wu, L. A. Zhang, X. Zhou, Y. Bu, W. Zhang, F. Chu, Y. Li, Y. Kong, Q. Zhang, *ACS Catal.* **2018**, *9*, 610.
- [139] S. Eissa, G. C. Jimenez, F. Mahvash, A. Guermoune, C. Tlili, T. Szkopek, M. Zourob, M. Siaj, *Nano Res.* **2015**, *8*, 1698.
- [140] J.-G. Yu, B.-Y. Yue, X.-W. Wu, Q. Liu, X.-Y. Jiang, M. Zhong, H.-Y. Li, S.-S. Li, X.-Q. Chen, *Curr. Org. Chem.* **2016**, *20*, 1284.
- [141] V. Georgakilas, M. Otyepka, A. B. Bourlino, V. Chandra, N. Kim, K. C. Kemp, P. Hobza, R. Zboril, K. S. Kim, *Chem. Rev.* **2012**, *112*, 6156.
- [142] B. N. Shivananju, L. Zhou, Y. Yin, W. Yu, B. Shabbir, H. Mu, X. Bao, Y. Zhang, S. Tian, Q. Ou, S. Li, M. M. Hossain, Y. Zhang, H. Shao, G. Xing, N. V. Medhekar, C. Li, J. Liu, Q. Bao, *InfoMat.* **2020**, *1*.

- [143] M.-Q. Yang, Y.-J. Xu, *Nanoscale Horiz.* **2016**, *1*, 185.
- [144] B. Wang, T. Ruan, Y. Chen, F. Jin, L. Peng, Y. Zhou, D. Wang, S. Dou, *Energy Storage Mater.* **2020**, *24*, 22.
- [145] X. Huang, X. Qi, F. Boey, H. Zhang, *Chem. Soc. Rev.* **2012**, *41*, 666.
- [146] B. Li, H. Cao, J. Shao, M. Qu, J. H. Warner, *J. Mater. Chem.* **2011**, *21*, 5069.
- [147] L. Yang, L. Wang, M. Xing, J. Lei, J. Zhang, *Appl. Catal., B* **2016**, *180*, 106.
- [148] D. Wu, W. Zhao, H. Wu, Z. Chen, H. Li, L. Y. Zhang, *Scr. Mater.* **2020**, *178*, 187.
- [149] J.-Q. Huang, J. Huang, W. G. Chong, J. Cui, S. Yao, B. Huang, J.-K. Kim, *J. Energy Chem.* **2019**, *35*, 204.
- [150] M. H. Zeb, B. Shabbir, R. U. R. Sagar, N. Mahmood, K. Chen, I. Qasim, M. I. Malik, W. Yu, M. M. Hossain, Z. Dai, *ACS Appl. Mater. Interfaces* **2019**, *11*, 19397.
- [151] P. Vecera, J. C. Chacón-Torres, T. Pichler, S. Reich, H. R. Soni, A. Görling, K. Edelhalmhammer, H. Peterlik, F. Hauke, A. Hirsch, *Nat. Commun.* **2017**, *8*, 15192.
- [152] K. Sampathkumar, V. Diez-Cabanes, P. Kovaricek, E. del Corro, M. Bouša, J. Hošek, M. Kalbac, O. Frank, *J. Phys. Chem. C* **2019**, *123*, 22397.
- [153] P. C. Santana, J. Lima, T. Santana, L. F. Santos, C. R. Matos, L. P. d. Costa, I. F. Gimenez, E. M. Sussuchi, *J. Braz. Chem. Soc.* **2019**, *30*, 1302.
- [154] I. A. Vacchi, C. Ménard-Moyon, A. Bianco, *Phys. Sci. Rev.* **2017**, *2*.
- [155] M. Del Cueto, P. Ocón, J. Poyato, *J. Phys. Chem. C* **2015**, *119*, 2004.
- [156] X. Bai, E. Zhao, K. Li, Y. Wang, M. Jiao, F. He, X. Sun, H. Sun, Z. Wu, *Carbon* **2016**, *105*, 214.
- [157] A. Kumatani, C. Miura, H. Kuramochi, T. Ohto, M. Wakisaka, Y. Nagata, H. Ida, Y. Takahashi, K. Hu, S. Jeong, *Adv. Sci.* **2019**, *6*, 1900119.
- [158] L. M. Rivera, S. Fajardo, M. D. C. Arévalo, G. García, E. Pastor, *Catalysts* **2017**, *7*, 278.
- [159] T. Zhang, C. He, F. Sun, Y. Ding, M. Wang, L. Peng, J. Wang, Y. Lin, *Sci. Rep.* **2017**, *7*, 43638.
- [160] X.-X. Xue, L.-M. Tang, K. Chen, L. Zhang, E.-G. Wang, Y. Feng, *J. Chem. Phys.* **2019**, *150*, 104701.
- [161] Y. Jiao, Y. Zheng, K. Davey, S.-Z. Qiao, *Nat. Energy* **2016**, *1*, 16130.
- [162] J. Lee, S. Noh, N. D. Pham, J. H. Shim, *Electrochim. Acta* **2019**, *313*, 1.
- [163] X. Zhang, Y. Wu, Y. Sun, P. Ding, Q. Liu, L. Tang, J. Guo, *Electrochim. Acta* **2018**, *263*, 140.
- [164] M. Li, Y. Wang, P. Tang, N. Xie, Y. Zhao, X. Liu, G. Hu, J. Xie, Y. Zhao, J. Tang, *Chem. Mater.* **2017**, *29*, 2769.
- [165] M. Sahoo, S. Ramaprabhu, *Carbon* **2018**, *127*, 627.
- [166] X. Chen, X.-R. Chen, T.-Z. Hou, B.-Q. Li, X.-B. Cheng, R. Zhang, Q. Zhang, *Sci. Adv.* **2019**, *5*, eaau7728.
- [167] H. An, Y. Li, Y. Gao, C. Cao, J. Han, Y. Feng, W. Feng, *Carbon* **2017**, *116*, 338.
- [168] X. Xiong, G. Wang, Y. Lin, Y. Wang, X. Ou, F. Zheng, C. Yang, J.-H. Wang, M. Liu, *ACS Nano* **2016**, *10*, 10953.
- [169] S. S. Balaji, M. Karnan, J. Kamarsamam, M. Sathish, *ChemElectroChem* **2019**, *6*, 1492.
- [170] D. M. El-Gendy, N. A. A. Ghany, N. K. Allam, *J. Electroanal. Chem.* **2019**, *837*, 30.
- [171] K. Kakaei, E. Alidoust, G. Ghadimi, *J. Alloys Compd.* **2018**, *735*, 1799.
- [172] P. Yan, L. Yan, S. Zhao, Z. Zuo, X. Wang, C. Wang, M. Hou, *Nano* **2019**, *14*, 1950099.
- [173] H. Deng, M. Zhu, T. Jin, C. Cheng, J. Zheng, Y. Qian, *Int. J. Electrochem. Sci.* **2020**, *15*, 16.
- [174] Q. Geng, G. Huang, Y. Liu, Y. Li, L. Liu, X. Yang, Q. Wang, C. Zhang, *Electrochim. Acta* **2019**, *298*, 1.
- [175] X. Bao, Q. Ou, Z. Q. Xu, Y. Zhang, Q. Bao, H. Zhang, *Adv. Mater. Technol.* **2018**, *3*, 1800072.
- [176] Z. Wang, Q. Ou, Y. Zhang, Q. Zhang, H. Y. Hoh, Q. J. Bao, *ACS Appl. Mater. Interfaces* **2018**, *10*, 24258.
- [177] K. P. Loh, Q. Bao, G. Eda, M. Chhowalla, *Nat. Chem.* **2010**, *2*, 1015.
- [178] Z. Dai, G. Hu, Q. Ou, L. Zhang, F. Xia, F. J. Garcia-Vidal, C.-W. Qiu, Q. Bao, *Chem. Rev.* **2020**, *120*, 6197.
- [179] P.-H. Shih, T.-N. Do, G. Gumbs, M.-F. Lin, *Phys. E* **2020**, *118*, 113894.
- [180] X. Dai, T. Shen, Y. Feng, H. Liu, *Phys. B* **2019**, *574*, 411660.
- [181] X. Dai, T. Shen, H. Liu, *Mater. Res. Express* **2019**, *6*, 085635.
- [182] X. Gan, R. Lv, T. Zhang, F. Zhang, M. Terrones, F. Kang, *Carbon* **2018**, *138*, 69.
- [183] K. Jayanand, S. Chugh, N. Adhikari, M. Min, L. Echegoyen, A. B. Kaul, *J. Mater. Chem. C* **2020**, *8*, 3970.
- [184] M. Gong, Q. Liu, R. Goul, D. Ewing, M. Casper, A. Stramel, A. Elliot, J. Z. Wu, *ACS Appl. Mater. Interfaces* **2017**, *9*, 27801.
- [185] H. Safardoust-Hojaghan, O. Amiri, M. Hassanpour, M. Panahi-Kalamuei, H. Moayedi, M. Salavati-Niasari, *Food Chem.* **2019**, *295*, 530.
- [186] Z. Ni, L. Ma, S. Du, Y. Xu, M. Yuan, H. Fang, Z. Wang, M. Xu, D. Li, J. Yang, *ACS Nano* **2017**, *11*, 9854.
- [187] M. Chen, C. Hou, D. Huo, J. Bao, H. Fa, C. Shen, *Biosens. Bioelectron.* **2016**, *85*, 684.
- [188] Y.-H. Wang, K.-J. Huang, X. Wu, Y.-Y. Ma, D.-L. Song, C.-Y. Du, S.-H. Chang, *J. Mater. Chem. B* **2018**, *6*, 2134.
- [189] K. Zhang, X. Chen, Z. Li, Y. Wang, S. Sun, T. Guo, D. Zhang, Z. Xue, X. Zhou, X. Lu, *Talanta* **2018**, *178*, 315.
- [190] H. Au, N. Rubio, M. S. Shaffer, *Chem. Sci.* **2018**, *9*, 209.
- [191] Z. Wei, Y. Chen, J. Wang, D. Su, M. Tang, S. Mao, Y. Wang, *ACS Catal.* **2016**, *6*, 5816.
- [192] A. Ariharan, B. Viswanathan, V. Nandhakumar, *Graphene* **2017**, *6*, 41.
- [193] Y. Ahn, H. Kim, Y.-H. Kim, Y. Yi, S.-I. Kim, *Appl. Phys. Lett.* **2013**, *102*, 091602.
- [194] V. P. Pham, K. N. Kim, M. H. Jeon, K. S. Kim, G. Y. Yeom, *Nanoscale* **2014**, *6*, 15301.
- [195] X. Li, L. Fan, Z. Li, K. Wang, M. Zhong, J. Wei, D. Wu, H. Zhu, *Adv. Energy Mater.* **2012**, *2*, 425.
- [196] W. S. Leong, G. Arrabito, G. Prestopino, *Crystals* **2020**, *10*, 308.
- [197] S. Zhang, S. Lin, X. Li, X. Liu, H. Wu, W. Xu, P. Wang, Z. Wu, H. Zhong, Z. Xu, *Nanoscale* **2016**, *8*, 226.
- [198] R. Lv, M. C. Dos Santos, C. Antonelli, S. Feng, K. Fujisawa, A. Berkdemir, R. Cruz-Silva, A. L. Elías, N. Perea-Lopez, F. López-Urías, *Adv. Mater.* **2014**, *26*, 7593.
- [199] B. Huet, J.-P. Raskin, *Carbon* **2018**, *129*, 270.
- [200] Y. Ito, C. Christodoulou, M. V. Nardi, N. Koch, H. Sachdev, K. Müllen, *ACS Nano* **2014**, *8*, 3337.
- [201] D. Wei, L. Peng, M. Li, H. Mao, T. Niu, C. Han, W. Chen, A. T. S. Wee, *ACS Nano* **2015**, *9*, 164.



**Sami Ullah** earned his M.Phil. degree from the Department of Chemistry at Quaid-i-Azam University, Islamabad, Pakistan, in 2016. Where his research was related to dye sensitized solar cells. Currently, he is a doctoral researcher at the Soochow Institute for Energy and Materials Innovations (SIEMIS) and the College of Energy at Soochow University China in Prof. Mark H. Rummeli's group. His present research direction is focused on the controlled development of chemically doped graphene by chemical vapor deposition and its applications.



**Nasir Mahmood Ahmad** is full professor and head of Polymer research Lab and Focal person of Polymer and Composites Research Group in School of Chemical and Materials Engineering, National University of Sciences and Technology (NUST), Islamabad. He has over 25-years extensive experiences both in academia and industry in the R & D of advanced materials and processes. He has been involved in studies, which include polymerization of acrylate, ethylene, and vinyl acetate monomers to manufacture primary resins, extrude plastic films and develop master batches.



**Mark H. Rummeli** heads the electron microscopy and LIN labs at the Soochow Institute for Energy and Materials Innovations (SIEMIS), Soochow University, where he is a full professor. He is also director of the characterization center at the College of Energy and SIEMES. He earned his Ph.D. from London Metropolitan University and then worked as a postdoc at the German Aerospace Center and the Leibniz Institute, the IFW-Dresden. His research focuses on the growth mechanisms of 2D nanostructures and their functionalization.